HOSTED BY

ELSEVIER

Available online at www.sciencedirect.com

ScienceDirect

Soils and Foundations 62 (2022) 101201

www.elsevier.com/locate/sandf

Technical Paper

New p-y model for seismic loading prediction of pile foundations in non-liquefiable and liquefiable soils considering modulus reduction and damping curves

Lilin Wang, Takeshi Ishihara *

Department of Civil Engineering, School of Engineering, The University of Tokyo, 7-3-1, Hongo, Bunkyo-ku, Tokyo, Japan

Received 12 January 2022; received in revised form 12 June 2022; accepted 4 July 2022

Abstract

In this study, a new p-y model is proposed for the seismic loading prediction of pile foundations using the Beam on Nonlinear Winkler Foundation (BNWF) method. It matches the desired modulus reduction curve by identifying three parameters in a hyperbolic function and a linear function using a genetic algorithm (GA), and the desired damping curve by applying the Ishihara-Yoshida rule that controls the unloading–reloading curves iteratively through the three parameters. The rate effect is integrated into the proposed PySimple5 model for clay by exerting influence on the ultimate capacity and maximum material damping through a power function, while the pore pressure effect is reflected in the proposed Pyliq5 model for sand by relating the ultimate capacity to the mean effective stress. For a single pile in non-liquefiable soil, the predicted superstructure acceleration and pile bending moment by PySimple5 agree well with those from centrifuge tests for different soil shear strain levels, while the equivalent linear and PySimple1 models underestimate them for soil shear strain levels higher than 1%. For a pile in liquefiable soil, PyLiq5 shows a reasonable agreement with the centrifuge tests in terms of the superstructure acceleration and pile bending moment by considering the pore pressure effect.

Keywords: Seismic loading; Pile foundation; PySimple5 and PyLiq5; Modulus reduction and damping curves; Rate effect; Pore pressure effect

1. Introduction

The accidental limit state (ALS) focuses on the damage caused by accidental hazards, such as earthquakes. As stated in DNVGL-RP-C212 (2017), it is necessary to consider the ALS in the design of support structures for wind turbines. In Japan, severe damage to such wind turbine support structures has occurred a few times in the past several years due to earthquakes. In 2011, during the East Japan earthquake, a wind turbine tower at the Kashima wind farm was tilted and its pile group foundation was cracked (Butt and Ishihara, 2012). In 2016, during the Kumamoto earthquake, a wind turbine tower at the Kugino wind farm buckled and all the pile group foundations of three wind turbines were damaged (Harukigaoka Wind Power Co., ltd., 2018). The Kashima wind farm is located on liquefiable reclaimed land, while the Kugino wind farm is located in a non-liquefiable mountainous area. Since soil-structure interaction plays an important role in the damage to wind turbines, it needs to be investigated.

The soil-structure interaction of pile foundations under severe earthquakes involves strong nonlinearities, including material nonlinearity and geometrical nonlinearity (e.g., soil-pile separation). There are two methods for considering the soil-structure interaction in the JSCE guideline

Peer review under responsibility of The Japanese Geotechnical Society.
* Corresponding author.
E-mail address: ishihara@bridge.t.u-tokyo.ac.jp (T. Ishihara).

https://doi.org/10.1016/j.sandf.2022.101201
0038-0806/

(Ishihara, 2010). One is the equivalent linear method with a one-dimensional model (hereafter referred to as the 1D model) for a maximum soil shear strain level of less than 1%, and the other is the nonlinear step-by-step method with a finite element analysis (FE analysis) for a maximum soil shear strain level of more than 1%. In addition, the modulus reduction and damping curves are used in both methods, as shown in the JSCE guideline (Ishihara, 2010). The modulus reduction and damping curves for clay are dependent on the plasticity index, while those for sand rely on the confining stress. In the equivalent linear 1D model, the nonlinear soil-structure interaction is captured by distributed springs and dashpots whose values are constant and obtained from the equivalent linear site response analysis. The FE analysis can consider the soil-pile interaction accurately, but is rarely used in the design of all the wind turbines at a wind farm, due to complexity of the model, computational effort, and laborious data processing.

The most widely used p-y models in analyses of piles include the American Petroleum Institute (API)'s sand model (API, 2010) and Matlock's model for clay (Matlock, 1970), which were proposed in the 1960s and 1970s for static and cyclic loading conditions. Earthquake-induced dynamic loading conditions were not considered in the formulation of these p-y models. Later, Boulanger et al. (1999) proposed a well-known p-y model, PySimple1, by calibrating to the API sand p-y model and Matlock's soft clay model. One appealing advantage of PySimple1 is that it can consider not only the material nonlinearity, but also the geometrical nonlinearity, since a gap model was included in PySimple1. However, it fails to match the modulus reduction curve because of a large linear portion in it. Due to the fact that a significant difference exists between the static and the dynamic p-y behavior, Choi et al. (2015) proposed a new p-y model for sand, PySimple3, following the principles of bounding surface plasticity. With a small linear range in PySimple3, it can yield a smooth modulus reduction curve, and the material constant C in it can control its backbone to appropriately match the desired modulus reduction curve. Choi et al. (2015) showed that PySimple3 can capture the nonlinear p-y behavior of piles in sand during earthquake loading much better than PySimple1. However, PySimple3 may overestimate the damping value for a large deformation and cannot capture the soil-pile separation behavior. Moreover, piecewise models, such as bilinear and trilinear models, have also been applied to model the soil-pile interaction (e.g., Krathe and Kaynia, 2017; Markou and Kaynia, 2018), but they cannot precisely reproduce the modulus reduction and damping curves.

The extended unloading–reloading Masing rules are usually utilized for existing p-y curves to model the hysteretic behavior of soil. This means that, at very small strain levels, the response is nearly linear and hysteretic damping is assumed to be small. However, this formulation can result in the significant overestimation of the damping ratio at large strain levels. PySimple1 and PySimple3 use different unloading-reloading rules that are based on the concept of a reversal point. Unfortunately, the same problem is encountered as the Masing rules. In the ground response analysis field, some unloading–reloading rules were proposed to model the hysteretic behavior accurately. The Ishihara-Yoshida rule (Ishihara et al., 1985) was proposed to solve the overestimation of soil damping when using the extended unloading–reloading Masing rules to model the hysteretic behavior. Recently, a one-dimensional nonlinear soil model, ARCS, capable of reproducing the desired modulus reduction and damping curves, was proposed by Yniesta et al. (2017). The ARCS model matches the desired modulus reduction curve by fitting cubic splines to the implied stress–strain curve and matches the damping curve by utilizing a coordinate transformation. However, the above rules have not been implemented in p-y models for pile response analyses.

Existing p-y models for pile response analyses are typically formulated in a rate-independent framework. However, the rate effect can affect the p-y curve since soil behavior strongly depends on the strain rate during an earthquake, which can reach 100%/s (Yniesta and Janati-Idrissi, 2021). It has been found that both the initial stiffness and damping increase significantly along with a high strain rate (D'Onofrio et al., 1999) and that poor predictions of the soil response will occur if the soil properties are not adjusted to consider the strain rate effect (Afacan et al., 2014). Yniesta and Janati-Idrissi (2021) reviewed the existing stress–strain models for ground response analyses. They found that, although some models can successfully capture the strain rate effect on soil stiffness or strength (Maranha et al., 2016), no model can capture the strain rate effect on damping. They also proposed a viscoplastic model for one-dimensional ground response analyses to capture the strain-rate dependency of soils. In the pile response analysis field, Brown (2004) performed a laboratory study of the effect of the rate of loading on piles in clay and a field test on a pile in glacial clay to calibrate the findings of the laboratory study. He found that the rate-dependent behavior can be represented by the modification of the nonlinear rate law proposed by Randolph (1992). Later, Brown and Powell (2013) investigated different rapid load test analysis techniques in clay to model the rate effect. Hölscher et al. (2012) conducted rapid loading tests on piles in sand and reported that both the rate and pore pressure effects contribute to the increase in pile toe resistance. The rate effect is limited for piles in sand (less than 10%), but the pore pressure effect can reach about 30%. In addition, only the effect of pore pressure was observed at the unloading point. In summary, cohesive soils are more sensitive to the strain rate effect than granular materials (Yniesta and Janati-Idrissi, 2021). Other researches (Yoo et al., 2013; Choi et al., 2015) also found that the dynamic pile capacity is significantly larger than the static one. However, they did not quantify the mechanism behind this behavior. Instead, they proposed an empirical model to

predict the dynamic ultimate capacity directly by fitting the experimental data. Unfortunately, such a correction is inaccurate because it implies that the rate effect is constant throughout the tests and that only the ultimate capacity is affected.

For liquefiable soil, the generation of pore water pressure is a crucial factor in the triggering of liquefaction, and the generated pore water pressure consequently changes the p-y curve. Brandenberg et al. (2013) proposed PyLiq1 by incorporating the pore water pressure effect on the soil shear strength degradation based on PySimple1. PyLiq1 was validated by the centrifuge tests performed by Wilson (1998) for a nearly horizontal ground and by Brandenberg et al. (2005) for a sloped ground. They also stressed that dilatancy is an important driver of the peak bending moments in pile foundations. Dash et al. (2017) pointed out that the p-y curve for fully liquefied soil has a different shape than that for non-liquefied soil. It should be concave upward with practically zero initial stiffness up to a certain displacement, due to the loss of particle-to-particle contact, beyond which the stiffness increases due to the reengaging of the sand particles. They also presented a practical method for the construction of newly proposed p-y curves for liquefied soil from a typical ground profile. However, these p-y curves cannot accurately predict the seismic loading on pile foundations in layered non-liquefiable and liquefiable soils since they are paired with conventional p-y curves which are not suitable for non-liquefiable soil.

In this study, the seismic loading prediction of pile foundations is investigated using the BNWF method with a new p-y model for non-liquefiable and liquefiable soils. In Section 2, the new p-y model is proposed to reproduce the modulus reduction and damping curves. It considers the rate effect for clay and the pore pressure effect for sand. In Section 3, the proposed model is validated for a single pile in non-liquefiable soil and compared to the equivalent linear 1D model and the conventional p-y model. The proposed model for use in liquefiable soil and the impact of liquefaction on pile foundations are also investigated. Conclusions are given in Section 4.

2. New p-y model

A new p-y model is proposed in Section 2.1 to match the modulus reduction and damping curves and to consider the rate and pore pressure effects. The genetic algorithm (GA)-based identification for the backbone curve's relevant parameters and the Ishihara-Yoshida rule-based iteration for the unloading–reloading relevant parameters are described in Section 2.2. Integration of the rate and pore pressure effects in PySimple5 and PyLid5 are introduced in Section 2.3 and Section 2.4, respectively. A comparison of PySimple5 with previous models is discussed in Section 2.5.

2.1. Description of new p-y model

As illustrated in Fig. 1(a), the Beam on Nonlinear Winkler Foundation (BNWF) method is adopted for the dynamic analyses of pile supported structures in this study, in which a new p-y model, called PySimple5, is proposed for any soil shear strain levels. The configuration of PySimple5 is presented in Fig. 1(b); it consists of linear ($p^e - y^e$), hyperbolic ($p^p - y^p$), and gap ($p^g - y^g$) components in series, in which the gap component comprises a drag element ($p^d - y^g$) in parallel with a closure element ($p^c - y^g$). The governing equations of PySimple5 are expressed in Eqs. (1)-(11). The force and stiffness in the linear component (Eqs. (1)-(2)), in the hyperbolic component (Eqs. (3)-(4)), in the gap component (Eqs. (5)-(8)), and in the overall spring (Eqs. (9)-(10)) are presented briefly here. By properly selecting the parameter of C_d in Eq. (6), PySimple5 can simulate the conditions with and without the formation of a gap, as shown in Fig. 1(b). It should be noted that Eq. (3) shows that unloading and reloading are achieved by updating the reversal point (y_0^p, p_0) in the plastic component of PySimple5, which is different from the widely used Masing rule, but whose idea is similar. The Masing rule (Masing 1926) asserts that, if the force–displacement curve for a cyclically stabilized system at initial loading is described by $f(r,x) = 0$, where r is the restoring force corresponding to the displacement x of the system, then the unloading and reloading branches of the steady-state hysteretic response of the system are geometrically similar to the initial-loading curve, except for a twofold magnification, and are described by $f((r - r_0)/2, (x - x_0)/2) = 0$, where (x_0, r_0) is the load reversal point for that particular loading branch.

$$p^e = K^e y^e \tag{1}$$

$$K^e = \eta \frac{p_{ult}}{y_{50}} \tag{2}$$

$$p^p = B \cdot E \cdot p_{ult} - (B \cdot E \cdot p_{ult} - p_0)\left(\frac{A \cdot E \cdot c \cdot y_{50}}{A \cdot E \cdot c \cdot y_{50} + |y^p - y_0^p|}\right)^n \tag{3}$$

$$K^p = \frac{\partial p^p}{\partial y^p} = \frac{n \cdot sign(\dot{y})(B \cdot E \cdot p_{ult} - p_0)}{|y^p - y_0^p| + A \cdot E \cdot c \cdot y_{50}}\left[\left(\frac{A \cdot E \cdot c \cdot y_{50}}{|y^p - y_0^p| + A \cdot E \cdot c \cdot y_{50}}\right)^n\right] \tag{4}$$

$$p^g = p^d + p^c \tag{5}$$

$$p^d = C_d \cdot p_{ult} - (C_d \cdot p_{ult} - p_0^d)\left(\frac{y_{50}}{y_{50} + 2|y^g - y_0^g|}\right)^n \tag{6}$$

$$p^c = 1.8 \cdot p_{ult}\left[\frac{y_{50}}{y_{50} + 50(y_0^+ - y^g)} - \frac{y_{50}}{y_{50} - 50(y_0^- - y^g)}\right] \tag{7}$$

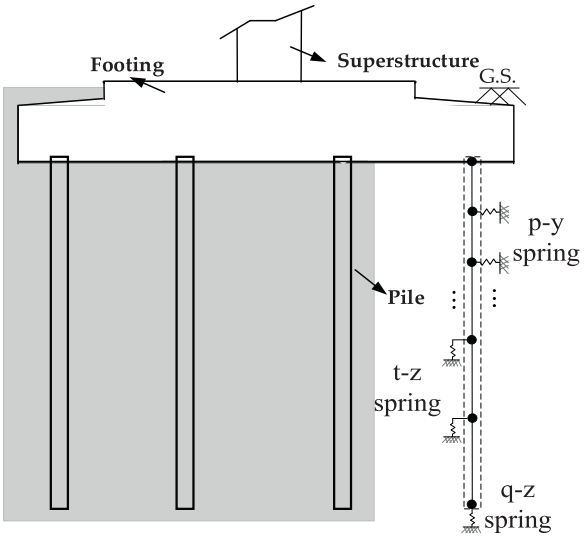

(a) Description of pile foundation supported by Winkler springs

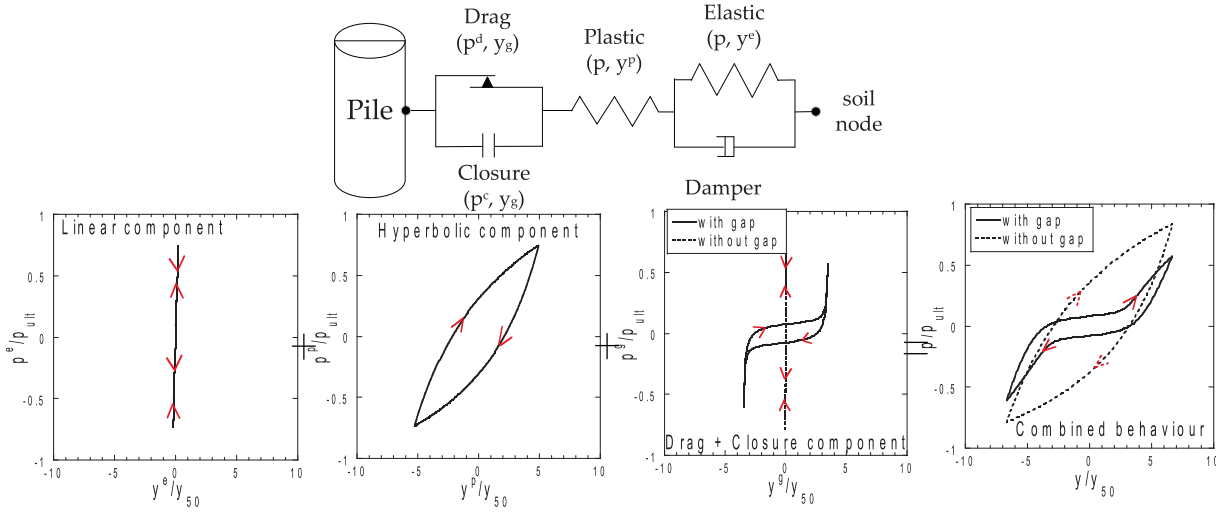

(b) Schematic of nonlinear p-y spring

Fig. 1. Beam on Nonlinear Winkler Foundation (BNWF) model with PySimple5.

$$K^g = \frac{\partial p^g}{\partial y^g} = \frac{2n\left(p_0^d - C_d p_{ult}\right)}{y_{50} + 2\left|y^g - y_0^g\right|}\left(\frac{y_{50}}{y_{50} + 2\left|y^g - y_0^g\right|}\right)^n + \frac{1.8 p_{ult}\frac{y_{50}}{50}}{\left(\frac{y_{50}}{50} - y^g + y_0^+\right)^2} + \frac{1.8 p_{ult}\frac{y_{50}}{50}}{\left(\frac{y_{50}}{50} + y^g - y_0^-\right)^2} \quad (8)$$

$$p = p^e = p^p = p^g \quad (9)$$

$$K = \left(1/K^e + 1/K^p + 1/K^g\right)^{-1} \quad (10)$$

$$f = |p - p_\alpha| - \left(C_r \cdot p_{ult}\right) \quad (11)$$

where K^e is the elastic modulus, K^p is the plastic modulus, K^g is the gap modulus, and K is the combined modulus. f is the yield function, p_α is the value of p at the center of the elastic region (analogous to the back stress in the classical plasticity theory), $C_r \cdot p_{ult}$ is the yielding force, and C_r is 0 in Pysimple5. This implies that the same model shape is used for both the inviscid part and the viscoplastic part, as defined by Gerolymos and Gazetas (2006) based on the Bouc–Wen model, and the hysteretic loop is established by using the same loading and unloading–reloading rule. The updating of the ultimate capacity is used to consider the rate effect, as mentioned by Brown (2004) and discussed in Section 2.3. The same idea is used, namely, updating the ultimate capacity to consider the pore pressure effect, as shown by Brandenberg et al. (2013) and discussed in Section 2.4. p_0 is the value of p at the start of the current plastic loading cycle and p_{ult} is the ultimate bearing capacity. y^e is the elastic component of the displacement, y^p is the plastic component of the displacement, y_0^p is the value of y_0 at the

start of the current plastic loading cycle, and y_{50} is the displacement where $p = 0.5p_{ult}$. p^d and p^c are the forces in the closure element and the drag element, respectively, and p_0^d is the value of p^d at the start of the current plastic loading cycle. y^g is the displacement across the gap element and y_0^g is the value of y^g at the start of the current plastic loading cycle. C_d is the ratio of the maximum drag force to the ultimate bearing capacity; it is set to 0.3, as given in Boulanger et al. (1999) according to the experiment. The gap component is used to capture the soil-pile separation, in which the drag element describes the friction from the side soil when the gap opens, while the closure element captures the closing of the gap when the pile touches the front soil. y_0^+ is the memory term for the positive side of the gap, while y_0^- is the memory term for the negative side of the gap. The initial values for y_0^+ and y_0^- are $y_{50}/100$ and $-y_{50}/100$, respectively. c, n, and η define the shape of the backbone curve of PySimple5, while A, B, and E determine the shape of unloading and reloading.

The parameters in PySimple5 can be divided into backbone curve relevant parameters (c, n, and η), unloading–reloading relevant parameters (A, B, and E), rate effect or pore pressure effect relevant parameters (p_{ult} and $h_{\max}$), and others (P_0, y_0^p, P_0^d, y_0^g, y_0^+ and y_0^-). The characteristics of PySimple5 include the reproduction of the desired modulus reduction and damping curves and consideration of the rate effect. Specifically, the backbone curve of PySimple5 is modelled as a hyperbolic function and a linear function in series, in which the three parameters, c, n, and η, are identified to fit the desired modulus reduction curve using GA. The unloading–reloading rule is modelled using the Ishihara-Yoshida rule with the three parameters, A, B, and E, that are iteratively determined to fit the desired damping curve. In addition, the rate effects that exert influence on the ultimate capacity (p_{ult}) and damping ($h_{\max}$) for clay are modelled using a power function where two parameters, α and β, are calculated using the findings by Sheahan et al. (1996) in which the percent of shear strength increase per logarithm of strain rate is constant. The pore pressure effects are reflected on the reduction in ultimate capacity (p_{ult}) through the mean effective stress.

2.2. Parameter identification

Zhang and Andersen (2017) developed static p-y curves by successfully scaling the site-specific soil stress–strain curves. Zhang et al. (2021) also validated their model for cyclic loading, and addressed a simplified damping model from the site-specific soil damping data using a finite element analysis (FEA). The same idea has also been used by Wang et al. (2020) and Lai et al. (2021). They concluded that the site-specific p-y curve outperforms the previous empirical formulations fitted to experimental data or a 3D FEA under certain soil conditions, since the applicability of these empirical formulations to certain soil conditions, other than those examined, is uncertain. This means that linking the p-y curve to the site-specific soil data, such as the stress–strain and damping-strain curves, is necessary for engineering applications on soil-pile interaction. However, Zhang et al. (2021) and Lai et al. (2021) relied on the concept of a nonlinear elastic model using springs and dashpots to implement the soil-pile interaction, which is a simplification of the hysteretic p-y curve proposed in this study. To illustrate the rationality of the proposed p-y model, a pseudo-static push-over analysis is performed in this study and shown in Appendix A.

In the present study, the backbone curve relevant parameters (c, n, and η) are identified by GA and goal seeking using the criterion that the backbone curve shall be capable of matching the desired modulus reduction curve. The fitness function of GA,$1/RMSE$, is defined as the ratio of the root mean squared error in Eq. (12), while the iteration will be stopped when Eq. (13) is satisfied or the generation reaches 50.

$$RMSE = \sqrt{\frac{1}{N}\sum_{i=1}^{N}\left(\frac{K_i}{K_0} - \frac{G_i}{G_0}\right)^2} \tag{12}$$

$$RMSE \leqslant 10^{-3} \text{ or } \phi_j - \phi_{j-1} \leqslant 10^{-3} \tag{13}$$

where $RMSE$ means the root mean square error. G_i is the modulus at the ith points of the modulus reduction curve, while K_i is the corresponding stiffness of the p-y curve. N is the number of points on the modulus reduction curve used for identification, which could be $10 \sim 20$ uniformly distributed points on the modulus reduction curve. G_0 and K_0 are the initial shear modulus and stiffness, respectively. ϕ_j means the parameter at the jth generation and ϕ could be c, n, or η.

One example of identifying c, n, and η by fitting to $G/G_0 = 1/(1 + \gamma/\gamma_{0.5})$ with $\gamma_{0.5} = 0.25\%$ is given here. The feature of PySimple5 is modelled using the zero-length beam element with input parameters, as described in Section 2.5. For the identification, the population is 50, the crossover probability is 0.9, the mutation probability is 0.09, and the generation stops at 50. The identified parameters are given in Table 1 and the RMSE in the identification procedure is shown in Fig. 2(a). The definitions of stiffness and damping, based on the hysteretic loop of PySimple5, are shown in Fig. 2(b). By exerting different displacements on the zero-length beam in Section 2.5, the relationships between stiffness or damping and displacement can be obtained. After that, the relationship between dis-

Table 1
Example of identified parameters for modulus reduction curve in H-D model.

Soil condition	Material constant	PySimple5
Clay or Sand	c	0.5
	n	0.7
	η	3.5

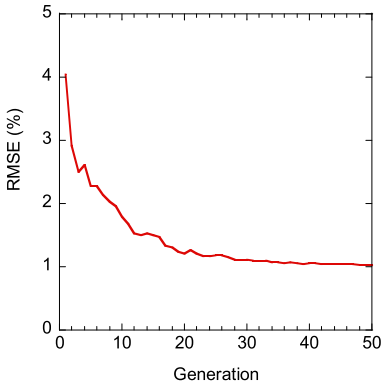

(a) RMSE in identification procedure

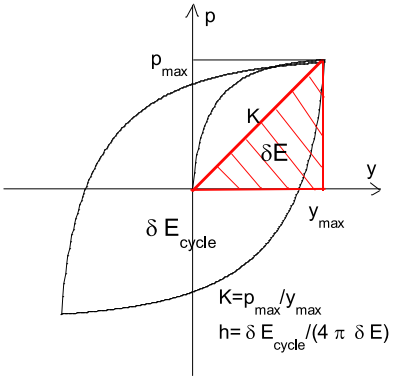

(b) Definitions of stiffness and damping

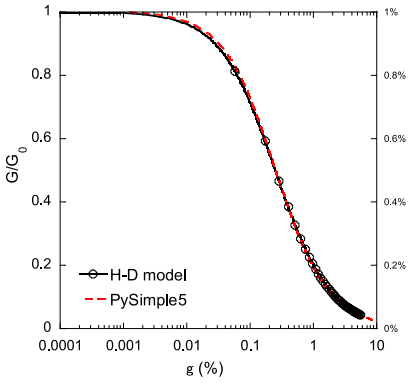

(c) Modulus reduction curve

Fig. 2. Example of PySimple5 backbone curve using parameters given in Table 1 and modulus reduction curve derived from PySimple5.

placement (y) and strain (γ), proposed by Kagawa and Kraft (1980), is used to convert displacement into strain, where $y = 2.5D\gamma$ and D is the pile diameter, and guarantees that $K/K_0 = 1/(1 + y/y_{50})$ and $h = h_{\max}y/(y_{50} + y)$ for the p-y curve corresponding to $G/G_0 = 1/(1 + \gamma/\gamma_{0.5})$ and $h = h_{\max}\gamma/(\gamma_{0.5} + \gamma)$ for the H-D model. The corresponding modulus reduction curve, using the parameters in Table 1, is portrayed in Fig. 2(c). It is observed that the proposed model matches the desired modulus reduction curve well.

The unloading–reloading relevant parameters (A, B, and E) can be updated using the Ishihara-Yoshida rule (Ishihara et al., 1985), following the criterion that the backbone curve shall be capable of matching the damping curve. The Ishihara-Yoshida rule was proposed for ground response analyses to solve the overestimation of soil damping when the soil strain is large. The Ishihara-Yoshida rule introduces three parameters in the original unloading/reloading rule and changes the hysteretic loop by dynamically updating the three parameters according to the desired damping curve. The same idea is used in this study for the p-y modelling. A, B, and E have different values for different loading conditions, as shown in Eq. (14), and are obtained iteratively to match the damping curve using Eqs. (15)-(17). It is noted that Eqs. (16)-(17) cannot be solved in a closed form for a_0 and e_0. They are solved numerically using the bisection method. The iteration will be stopped when Eq. (18) is satisfied or the number of iterations reaches 50. Eq. (9) is also examined, and the iteration will be stopped when Eq. (19) is satisfied or the number of iterations reaches 20.

$$\begin{cases} \text{skeleton curve:}, A = 1, B = 1, E = 1 \\ \text{unloading}: \ A = a_0, B = b_0, E = 1 \\ \text{reloading} \quad \text{reunloading}: \ A = a_0, B = b_0, E = e_0 \end{cases} \tag{14}$$

$$b_0 = \frac{\left(\frac{c \cdot y_{50}}{c \cdot y_{50} + \left|y_0^p\right|}\right)^n - 1}{\left(\frac{a_0 \cdot c \cdot y_{50}}{a_0 \cdot c \cdot y_{50} + \left|y_0^p\right|}\right)^n - 1} \tag{15}$$

$$L(a_0) = D\left(\frac{y_{0i}^p}{a_0}\right) - h(y_{0i}^p) = 0 \tag{16}$$

$$M(e_0) = f\left(\frac{y_{0i}^p}{a_0}\right) - \frac{p_{0i}/b_0}{e_0} = 0 \tag{17}$$

Here,

$h(y) = h_{\max}\left(\frac{y}{y_{50}+y}\right), D(y) = \frac{1}{4\pi}\frac{\Delta W(y)}{W(y)}, W(y) = \frac{1}{2}y \cdot g(y),$

$\Delta W(y) = 2\int_{-y}^{y} g(y_0)dy_0,$-

$$g(y)=\begin{cases} p_{ult}-(p_{ult}-p_{0i}/b_0)\left(\frac{c\cdot y_{50}}{c\cdot y_{50}+\left(y-y^p_{0i}/a_0\right)}\right)^n & (\Delta y>0)\\ -p_{ult}+(p_{ult}+p_{0i}/b_0)\left(\frac{c\cdot y_{50}}{c\cdot y_{50}-\left(y-y^p_{0i}/a_0\right)}\right)^n & (\Delta y<0)\end{cases}$$

$$f(y)=\begin{cases} p_{ult}-\left(p_{ult}-\frac{p_{0i+1}/b_0}{e_0}\right)\left(\frac{c\cdot y_{50}}{c\cdot y_{50}+\left(\frac{y-y^p_{0i+1}/a_0}{e_0}\right)}\right)^n & (\Delta y>0)\\ -p_{ult}+\left(p_{ult}+\frac{p_{0i+1}/b_0}{e_0}\right)\left(\frac{c\cdot y_{50}}{c\cdot y_{50}-\left(\frac{y-y^p_{0i+1}/a_0}{e_0}\right)}\right)^n & (\Delta y<0)\end{cases}$$

where $h(y)$ is the desired damping curve. $D(y)$ represents the damping corresponding to the $p-y$ loops. $\Delta W(y)$ is the damping energy and $W(y)$ is the equivalent elastic strain energy. Coordinates $(y^p_{0i},\ p_{0i})$ and $(y^p_{0i+1},\ p_{0i+1})$ are the most recent two reversal points.

$$\text{abs}\left(D\left(\frac{y^p_{0i}}{a_0}\right)-h(y^p_{0i})\right)/h(y^p_{0i})\leqslant 1.0e^{-3}$$
$$or\ \text{abs}\left(D\left(\frac{y^p_{0i}}{a_0}\right)-h(y^p_{0i})\right)\leqslant 1.0e^{-3} \quad (18)$$

$$\text{abs}\left(f\left(\frac{y^p_{0i}}{a_0}\right)-\frac{p_{0i}/b_0}{e_0}\right)/\frac{p_{0i}/b_0}{e_0}\leqslant 1.0e^{-3}$$
$$or\ \text{abs}\left(f\left(\frac{y^p_{0i}}{a_0}\right)-\frac{p_{0i}/b_0}{e_0}\right)\leqslant 1.0e^{-3} \quad (19)$$

$$\frac{3p-p^e-p^p-p^g}{p_{\text{ult}}}\leqslant 1.0e^{-12} \quad (20)$$

PySimple5 is implemented in OpenSees (Mazzoni et al., 2006) and solved iteratively when it is applied to dynamic analyses of pile supported structures. The flow chart in Fig. 3 shows how the parameters in PySimple5 are determined and how PySimple5 is solved iteratively in OpenSees.

2.3. Integration of rate effect in PySimple5 for clay

The rate effect relevant parameters, p_{ult} and $h_{\max}$, are calculated based on a rate effect model. For the ground response analysis, Yniesta and Janati-Idrissi (2021) proposed a viscoplastic model by adding viscous stress, that is directly strain-rate dependent, to the inviscid stress. Their model is consistent with the findings by Sheahan et al. (1996), namely, that the percent of shear strength increase per logarithm of strain rate is constant. However, a limitation of their model is that the damping response is not quantitatively controlled. In this study, viscoplasticity is achieved by multiplying a rate effect model to p_{static}, as shown in Eq. (21), where p_{static} represents the inviscid p-y reaction from the model proposed above and $R(\dot{y})$ is a rate effect model similar to that presented in Brown (2004). Eq. (21) can be achieved more conveniently using Eqs. (22)-(23), which relate the rate effect to the ultimate capacity and maximum damping as well as the static values obtained from the static load tests.

$$p=p_{static}+\Delta p=p_{static}R(\dot{y}) \quad (21)$$
$$p_{ult}=(p_{ult})_{static}+\Delta p_{ult}=(p_{ult})_{static}R(\dot{y}) \quad (22)$$
$$h_{\max}=(h_{\max})_{static}+\Delta h_{\max}=(h_{\max})_{static}R(\dot{y}) \quad (23)$$

Here, $R(\dot{y})=1+\alpha(\dot{y})^{\beta}$

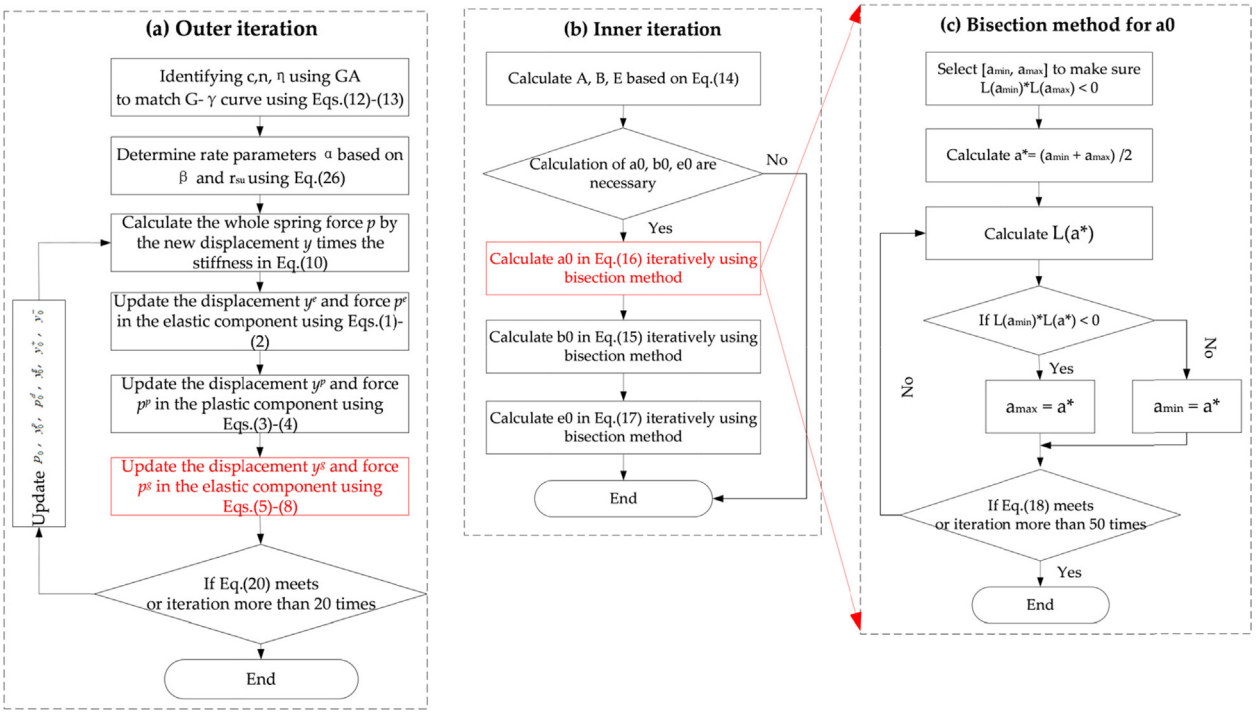

Fig. 3. Flow chart for determining parameters in PySimple5.

where p is the reaction of the p-y model at an elevated penetration rate, p_{static} is the reaction of the p-y model at a low penetration rate, similar to those encountered during static pile testing, $\dot{y}$ is the relative pile-soil slip velocity, and α and β are rate parameters.

Sheahan et al. (1996) observed that the shear strength increases with the strain rate. Rate parameters α and β shall be specifically determined so that the response of the model will be consistent with the study by Sheahan et al. (1996). Referring to Yniesta and Janati-Idrissi (2021), β is set as a value between 1/10 to 1/6. α can be derived based on the desired increase in shear strength per logarithmic cycle of shear strain rate, called r_{su}, with an average increase of 5%-20% per logarithmic cycle of strain rate. The definition for α as a function of r_{su} is demonstrated below.

It is assumed that a single p-y element is monotonically loaded at a constant displacement rate of 1 m/s up to a deformation of 1 m. Based on Eq. (21), the total force can be computed as Eq. (24). If another test is done at the slower rate of 10^{-5} m/s, p_1 can be defined and the total force reaches the deformation of 1 m, as given by Eq. (25).

$$p(1\text{m}) = p_{\text{static}}(1\text{m}) \cdot R(1\text{m/s}) \tag{24}$$

$$p_1(1\text{m}) = p_{\text{static}}(1\text{m}) \cdot R\left(10^{-5}\text{m/s}\right) \tag{25}$$

The ratio $p(1\text{m})/p_1(1\text{m})$ depends on the desired increase r_{su} in shear strength per logarithmic cycle of strain rate and, because there are six logarithmic cycles between 10^{-5} m/s and 1 m/s, this ratio can be presented as Eq. (26). α can be computed as a function of r_{su} and expressed as Eq. (27). It is noted that 10^{-5} m/s is selected because the static ultimate capacity is usually defined as 10^{-5} m/s (see Brown, 2004).

$$\begin{aligned}(1+r_{su})^6 &= \frac{p_{\text{static}}(1\text{m}) \cdot R(1\text{m/s})}{p_{\text{static}}(1\text{m}) \cdot R\left(10^{-5}\text{m/s}\right)} \\ &= \frac{p_{\text{static}}(1\text{m}) \cdot \left[1+\alpha(1\text{m/s})^{\beta}\right]}{p_{\text{static}}(1\text{m}) \cdot \left[1+\alpha\left(10^{-5}\text{m/s}\right)^{\beta}\right]}\end{aligned} \tag{26}$$

$$\alpha = \frac{(1+r_{su})^6 - 1}{(1\text{m})^{\beta} - \left(10^{-5}\text{m/s}\right)^{\beta}(1+r_{su})^6} \tag{27}$$

2.4. Integration of pore pressure effect in PyLid5 for sand

The PyLiq1 model was proposed by Brandenberg et al. (2013) to model the liquefiable soil-pile interaction by inputting the ground motion and mean effective stress time series from a free-field soil column to the free end of PySimple1. The only difference between PyLiq1 and PySimple1 is that the ultimate capacity of the p-y material, p_{ult_liq}, is treated as a variable that depends on the mean effective stress in the free field, σ', rather than being specified as a material constant. PySimple5 can consider the pore pressure effect using the same idea, which is named PyLiq5. All the parameters in PyLiq5 are the same as those in PySimple5, except for the ultimate bearing capacity,p_{ult_liq}, that is given as.

$$p_{ult\_liq} = p_{res} + (p_{ult} - p_{res})\frac{\sigma'}{\sigma'_0} \tag{28}$$

where σ'_0 is the initial free-field effective stress. It is shown that the value of p_{ult_liq} depends on the pore water pressure that develops in the free field and finally reaches a residual value p_{res} when σ' equals zero. A p-multiplier approach was introduced to clarify the residual capacity as $p_{res} = m_p \cdot p_{ult}$, where m_p was defined based on Brandenberg et al. (2005).

The ground motion and mean effective stress are input to the free ends of the PyLiq1 elements, as demonstrated in Fig. 4. The developed PyLiq5 model possesses the same advantages and disadvantages as PyLiq1. As expressed in Brandenberg et al. (2013), the material is also capable of modeling the transient stiffening associated with the cyclic mobility behavior of sand in cyclic undrained loading. The dilatancy induced by the local strain imposed on the soil by the pile can be indirectly incorporated by specifying an appropriate value for p_{res}. However, the concave upward p-y behavior and the inverted cone-shaped negative pore water pressure region around the pile are not included in the PyLiq5 model for simplification.

2.5. Comparison of proposed and conventional models

A comparison is performed to investigate the performance of PySimple5, PySimple3, and PySimple1 to match with the modulus reduction and damping curves. It should be noted that the rate and pore pressure effects in PySimple5 and Pyliq5 are not discussed here. It is assumed that

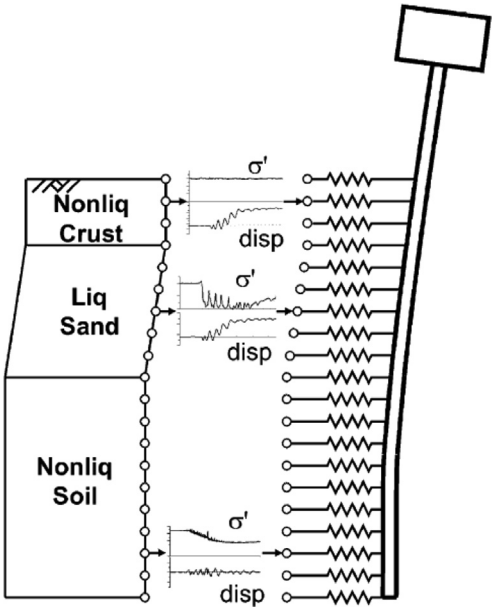

Fig. 4. Schematic of ground motion and mean effective stress from site response analysis input to free ends of PyLiq1 elements (Brandenberg et al., 2013).

PySimple5 is assigned to a zero-length beam element cyclically subject to a unit axial force with the input parameters $p_{ult} = 1$, $D = 1$, and $C_d = 10$, as shown in Fig. 5(a), to fit the H-D model with parameters $\gamma_{0.5} = 0.25\%$ and $h_{\max} = 20\%$. y_{50} is calculated by $y_{50} = 2.5D\gamma_{0.5}$ and equal to 0.625%. The beam element is fixed at one node and free at the other node. OpenSees has defined its own methods for analysis. The constraint handler determines how the constraint equations are enforced in the analysis; the numberer determines the mapping between the equation numbers and the degrees-of-freedom; the integrator determines the predictive step for time $t + dt$; the algorithm determines the sequence of steps taken to solve the nonlinear equation at the current time step; the system specifies how to store and solve the system of equations in the analysis; and the convergence determines when convergence has been achieved. More information can be found in Mazzoni et al. (2006). The analysis is conducted using the penalty method for the constraint handler, the reverse Cuthill-McKee scheme for the numberer, and the displacement control method for the integrator. The convergence tolerance on the energy unbalance in the system is 10^{-6}. Fig. 5 (b) illustrates the load–displacement responses (also known as the hysteresis loops) of PySimple5, PySimple3, and PySimple1. It is seen that the hysteresis loop for PySimple5 is different from the loops for PySimple3 and PySimple1. The modulus reduction and damping curves of PySimple5, PySimple3, and PySimple1 are derived from load-displacement curves and compared in Fig. 6. It is observed that PySimple5 matches well with the target modulus reduction and damping curves described by $G/G_0 = 1/(1 + \gamma/\gamma_{0.5})$ and $h = h_{\max}\gamma/(\gamma_{0.5} + \gamma)$ with $\gamma_{0.5} = 0.25\%$ and $h_{\max} = 20\%$. However, PySimple3 overestimates damping at large strain levels and PySimple1 fails to capture the modulus reduction and damping curves. More specifically, PySimple1 does not output a smooth modulus reduction curve due to the initial range in rigid behavior of the plastic component. It underestimates the

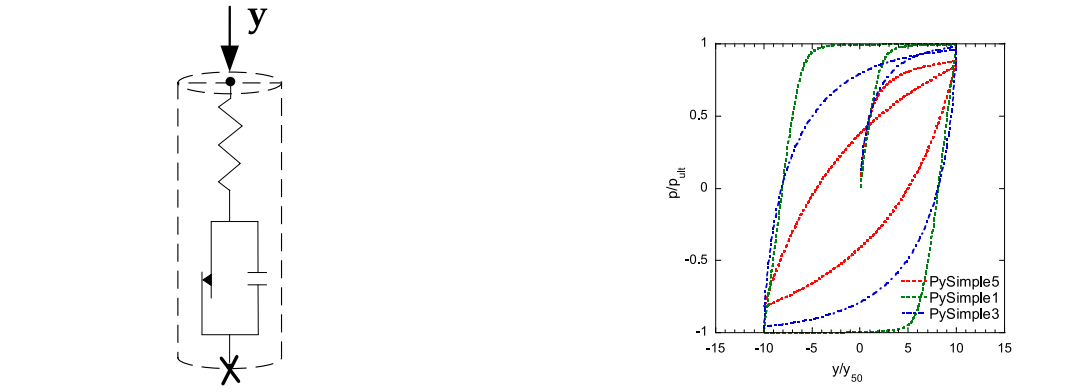

Fig. 5. Zero-length beam element with PySimple5 and normalized hysteresis loops.

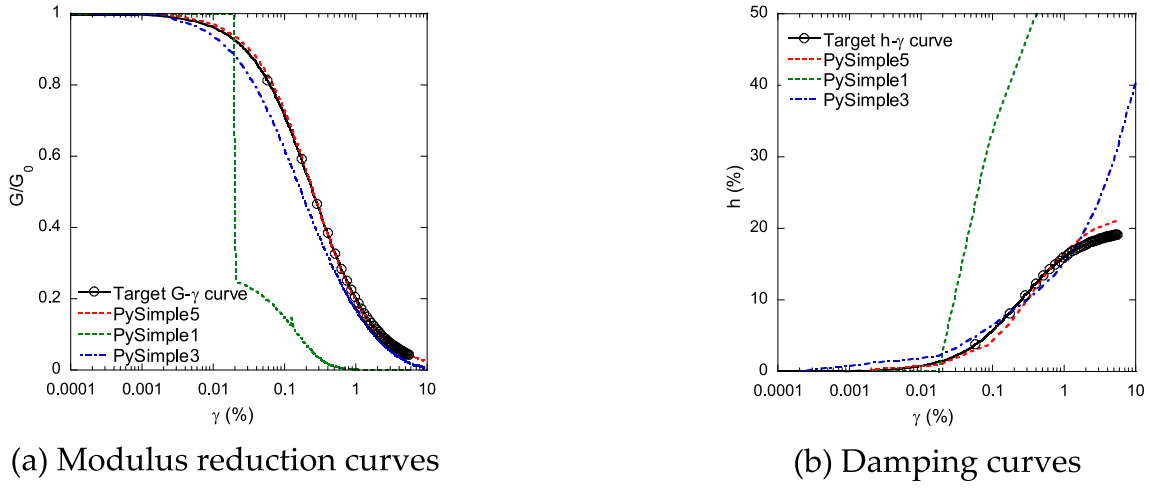

Fig. 6. Comparisons of modulus reduction and damping curves among PySimple1, PySimple3, and PySimple5.

soil damping at small strain levels, but significantly overestimates the soil damping at large strain levels due to its unloading and reloading rules.

Table 2 summarizes characteristics among Pysimple1, Pysimple3, and Pysimple5. Pysimple5 matches the modulus reduction and damping curves by identifying parameters c, n, and η in Eqs. (2)-(3) and A, B, and E in Eq. (4). This model also considers the rate and pore pressure effects, as discussed in Sections 2.3 and 2.4, as well as the soil-pile separation behavior using Eqs. (5)-(8). It indicates that Pysimple5 and PyLiq5 can consider the nonlinear and dynamic effects of soil and can be used for both non-liquefiable and liquefiable soils. Pysimple1, as mentioned in Brandenberg et al. (2013), cannot match the modulus reduction and damping curves, as shown Fig. 6, since parameters c, n, and η in Eqs. (2)-(3) are fixed for sand and clay, and constant values of $C_r = 0.35$ and $C_r = 0.2$ are used in Eq. (11) for clay and sand in Pysimple1, which result in a wide elastic region, as shown in Fig. 6(a). Parameters A,B, and E in Eq. (4) are 1 in Pysimple1, which cause the underestimation of damping in the small strain region and the overestimation of damping in the large strain region, which can be seen from Fig. 6 (b). Pysimple1 can simulate the soil-pile separation behavior using Eqs. (5)-(8). However, it cannot consider the rate effect, which leads to the underestimation of the acceleration responses of superstructures and the bending moments of piles for seismic loading predictions, as mentioned in Section 3. Pysimple3 favorably matches the modulus reduction curve as shown in Fig. 6 (a), since the material constant C in it can control its backbone to match with the desired modulus reduction curve, as shown Choi et al. (2015), which results in a narrow elastic region. Pysimple3 also overestimates the damping in the large strain region, as shown in Fig. 6 (b), since it cannot match the damping curves either. Pysimple3 uses the dynamic ultimate capacity by fitting the results from the centrifuge tests, which implies that it cannot be used for cases without experimental data. Moreover, Pysimple3 cannot capture the soil-pile separation behavior since Eqs. (5)-(8) are not used in this model. Piecewise models, such as bilinear and trilinear models, are discontinuous functions and can reproduce the modulus reduction and damping curves only at two or three points. They are unable to consider the rate or pore pressure effects or the soil-pile separation behavior for the seismic loading predictions of pile foundations. It should be noted that PySimple5 can return to PySimple1 as long as the backbone parameters are the same as PySimple1 ($C_r = 0.35$, $c = 10.0$, $n = 5.0$, and $\eta = 1.02$ for clay and $C_r = 0.2$, $c = 0.5$, $n = 0.5$, $\eta = 0.54$ for sand) and the Ishihara-Yoshida rule is not used ($A = B = E = 1.0$), which means that PySimple5 can match the classical API model well since PySimple1 was calibrated by the API model. In summation, PySimple5 outperforms the classical p-y curves since PySimple5 is suitable for various soil conditions, while the classical p-y curves fitted for certain soil conditions may not work well for other soil conditions.

Table 2
Comparison of characteristics among Pysimple1, Pysimple3, and Pysimple5.

Characteristic	Pysimple1 and PyLid1	Pysimple3	Pysimple5 and PyLid5
Modulus reduction curve	–	+	+
Damping curve	–	–	+
Rate effect or dynamic effect	–	+	+
Pore pressure effect	+	–	+
Soil-pile separation behavior	+	–	+

Note: "+" or "-" means that this characteristic is included or not.

3. Validation of proposed PySimple5 and PyLiq 5 for single pile

The proposed model for non-liquefiable soil, PySimple5, is firstly validated in Section 3.1 and then compared to the conventional methods in Section 3.2. Finally, the proposed model for liquefiable soil, PyLiq5, is validated for a single pile in liquefiable soil in Section 3.3.

3.1. Validation of PySimple5 for single pile in non-liquefiable soil

The centrifuge tests in Wilson (1998) for a single pile in soft clay are selected to validate the proposed model, which are referred to as CSP5 Event A and Event C. A schematic of the tests is shown in Fig. 7. The soil profile consisted of a top layer of saturated soft clay and a bottom layer of saturated dense sand. The depths of the clay and sand layers were 6.0 m and 11.4 m, respectively. In terms of the soil properties, the undrained shear strength of the clay was 2.5, 6.5, 9.0, and 12.0 kPa at depths of 0-1.5, 1.5-3.0, 3-4.5, and 4.5-6.0 m, respectively, while the friction angle of the sand was 3.95°. The effective unit weights of the clay and sand were $7.75kN/m^3$ and $9.81kN/m^3$, respectively. The soil parameters for the clay and sand in the CSP5 test are summarized in Table 3, where the low shear strain modulus of the clay in the Wilson test was derived from the available Torvane measurements using the equation $G = 200c_u$, where c_u is the undrained shear strength (Bowles, 1993). The parameters of the underlying sandy layer were extracted from the values reported by Popescu and Prevost (1993) for Nevada sand with Dr = 80%. The single pile was equivalent to a steel pipe pile with a diameter of 67 cm, a wall thickness of 1.9 cm, and an embedded length of about 16.5 m in the prototype scale, which was extended 3.8 m above the ground surface to carry a superstructure with a weight of 49 t (480.2 kN). The imposed excitations at the model base were the scaled Santa Cruz seismic waves with amplitudes of 0.035 g for Event A and 0.3 g for Event C, as shown in Fig. 8. In this section, the damping issues are addressed following Wang and Ishihara (2020), more specifically, the hysteretic damping is captured by PySimple5, the small-strain damping is incorporated into the

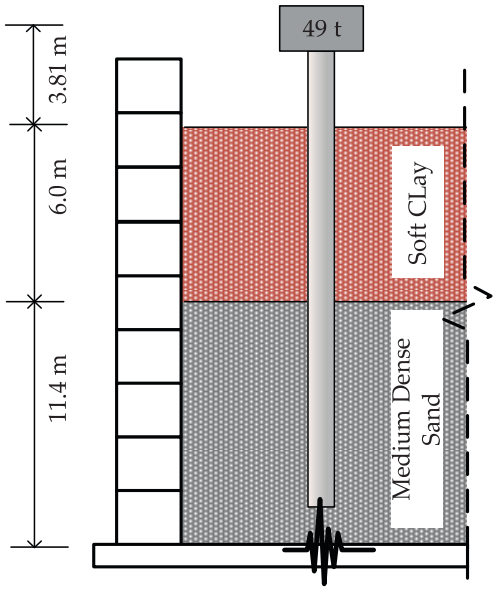

Fig. 7. Schematic of CSP5 centrifuge tests (after Wilson,1998).

Table 3
Soil parameters of CSP5 centrifuge tests.

	Clay (0–1.5 m)	Clay (1.5–3 m)	Clay (3–4.5 m)	Clay (4.5–6 m)	Sand
G_r(MPa)	0.5	1.3	1.8	2.4	41.5
B_r(MPa)	2.33	6.1	8.4	11.2	90.0
c_u(kPa)	2.5	6.5	9.0	12.0	0.0
ϕ(degree)	0.0	0.0	0.0	0.0	39.5

Note:G_r, low-strain shear modulus;B_r, low-strain bulk modulus;c_u, undrained shear strength;ϕ, soil friction angle.

structural damping, and the radiation damping is not considered in order to maintain consistency with Choi et al. (2015). The structural damping is modelled as Rayleigh damping with a value of 2% for both first and second modes (IEC61400-6, 2000). The same method is used for the whole paper and is not mentioned again elsewhere.

As shown in Afacan et al. (2014), the modulus reduction and damping curves, described by the H-D model with parameters $\gamma_{0.5} = 0.15\%$, $h_{max} = 21\%$, are used for the bay mud. Following Yniesta and Janati-Idrissi (2021), the modulus reduction, corrected for the monotonic shear strength, but not for the strain rate, shall be used since the strain-rate dependency is included directly in the proposed model. The modulus reduction and damping curves for Nevada sand are assumed to follow the H-D model with parameters $\gamma_{0.5} = 0.1\%$, $h_{max} = 21\%$. The desired increase in shear strength per logarithmic cycle of strain rate, r_{su}, is set at 13% for all clay layers ($\alpha = 1.57, \beta = 1/6$), to be consistent with the observations from the laboratory tests (Afacan et al., 2019).

The seismic soil-pile interaction analysis includes the site response analysis and the pile response analysis (Matlock et al., 1978). As illustrated in Fig. 9, the site response analysis is performed to obtain depth-dependent ground motion time histories along the pile that will be applied to the supports of the nonlinear springs for the pile response analysis. As shown in Boulanger et al. (1999), the accuracy of the pile response analysis would be reduced due to differences between the recorded and the calculated site responses. Therefore, the site response analysis shall be performed accurately. In this study, the site response analysis is performed using PressureIndependMultiYield material (PUDY) for clay in OpenSees and PressureDependMultiYield material (PMDY) for sand with parameters, as shown in Table 4 following Rahmani et al. (2018). The calculations of the ultimate capacity for clay follow DNVGL-RP-C212 (2017) and those for sand use the formulae in Gerolymos and Gazetas (2006). A series of site response analyses is performed for Event A and Event C. It is found that the maximum soil shear strain (γ_{max}) is 0.9% for Event A and 9.1% for Event C. Fig. 10 illustrates the predicted and measured acceleration responses at the depth of 1.6 m.

The pile response analysis is carried out using the Beam on Nonlinear Winkler Foundation (BNWF) method with PySimple5, as shown in Figs. 11-12. It is seen that the acceleration responses of the superstructure are underesti-

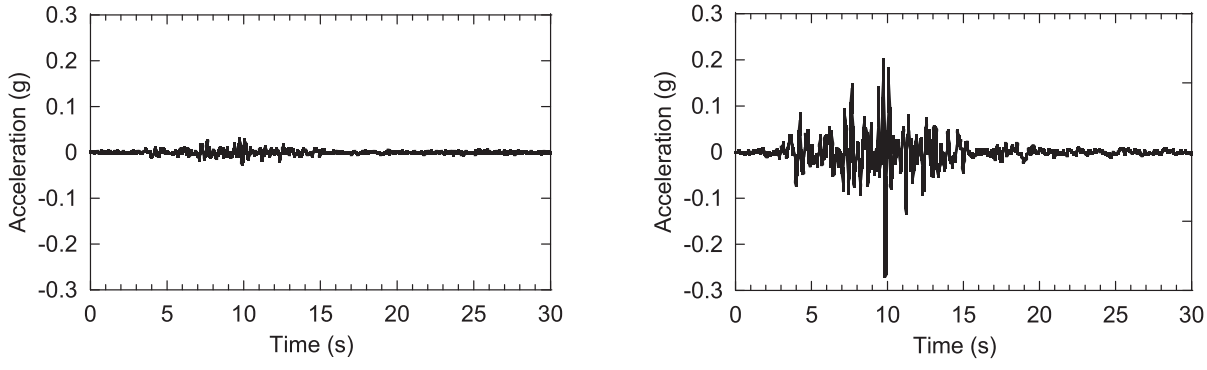

(a) Event A (0.035g) (b) Event C (0.30g)

Fig. 8. Time histories of imposed acceleration in CSP5 centrifuge tests.

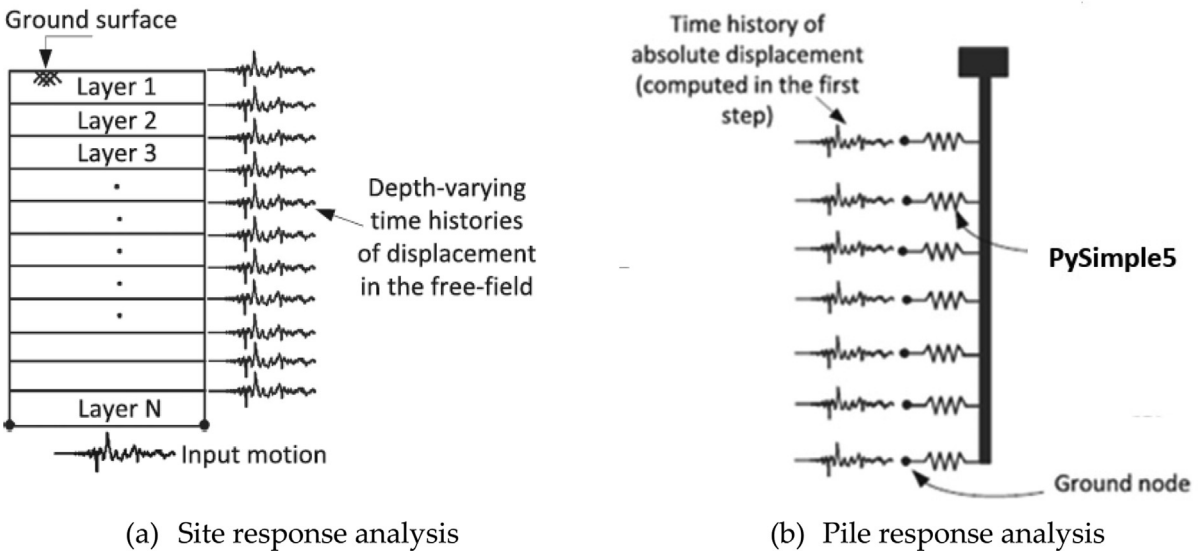

Fig. 9. Schematics of seismic soil-pile interaction analysis with p-y springs (after Rahmani et al., 2018).

mated by PySimple5 without the rate effect for either event, while PySimple5 with the rate effect gives slightly conservative results. This is because the rate effect increases the dynamic stiffness of the soil and results in an increase in the acceleration responses of the superstructure. Figs. 13-14 show the predicted and measured bending moment responses of the pile at the instance of the maximum pile displacement by PySimple5. It is observed that PySimple5 with the rate effect improves the accuracy of the predictions, while PySimple5 without the rate effect underestimates the bending moment of the pile near the ground surface since the maximum pile displacements are underestimated due to the underestimation of the ultimate bearing capacity, as shown in Eq. (22). The rate effect also significantly affects the maximum bending moment of the single pile, according to the simulation results in this study, as Yniesta and Janati-Idrissi (2021) showed that it did exert great influence on the site responses.

3.2. Comparison of proposed and conventional models for single pile in non-liquefiable soil

The equivalent linear 1D model is widely used in engineering practice, when the maximum soil shear strain is less than 1%, as shown in the JSCE guideline (Ishihara, 2010).

Table 4
Parameters of PDMY and PIMY for simulating soil behavior in dynamic centrifuge tests (after Rahmani et al., 2018).

Parameter	CSP5 test				
	Clay (0–1.5 m)	Clay (1.5–3 m)	Clay (3–4.5 m)	Clay (4.5–6 m)	Sand
G_r(MPa)	0.5	1.3	1.8	2.4	41.5
B_r(MPa)	2.33	6.1	8.4	11.2	90.0
c_u(kPa)	2.5	6.5	9.0	12.0	0.0
ϕ(degree)	0.0	0.0	0.0	0.0	39.5
γ_{max}	0.1	0.1	0.1	0.1	0.1
ϕ_{PT}(degree)	–	–	–	–	27.0
n	–	–	–	–	0.5
$d1$	–	–	–	–	0.6
$d2$	–	–	–	–	3.0
c	–	–	–	–	0.05

Note: G_r, low-strain shear modulus; B_r, low-strain bulk modulus; c_u, undrained shear strength; γ_{max}, octahedral shear strain at which maximum shear strength is reached; n, constant defining variation in shear modulus as function of mean effective confinement; ϕ, soil friction angle; ϕ_{PT}, phase transformation angle; $d1$ and $d2$, dilation parameters; c, contraction parameter.

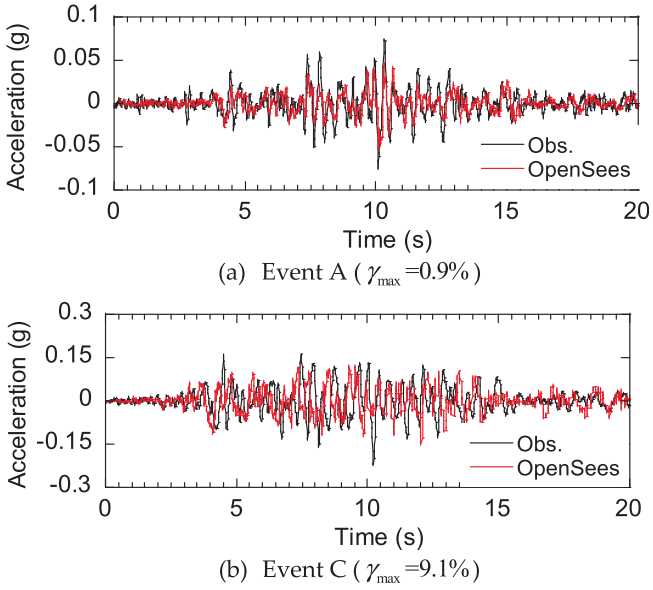

Fig. 10. Comparisons of measured and predicted acceleration time histories.

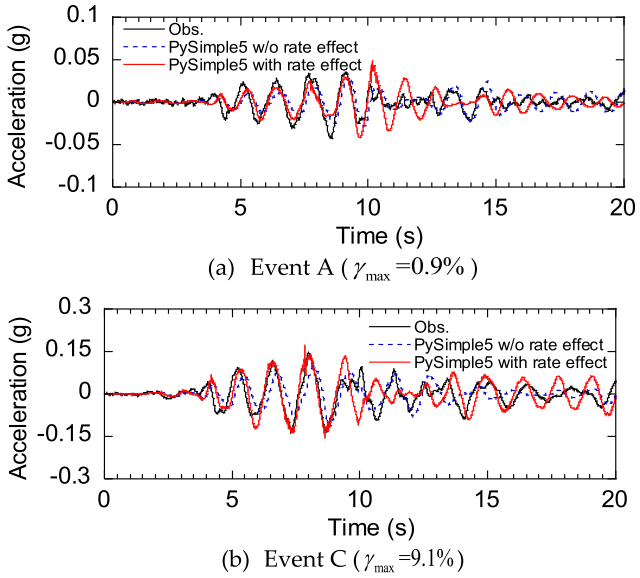

Fig. 11. Comparisons of measured and predicted acceleration time histories of superstructure with damping of 5%.

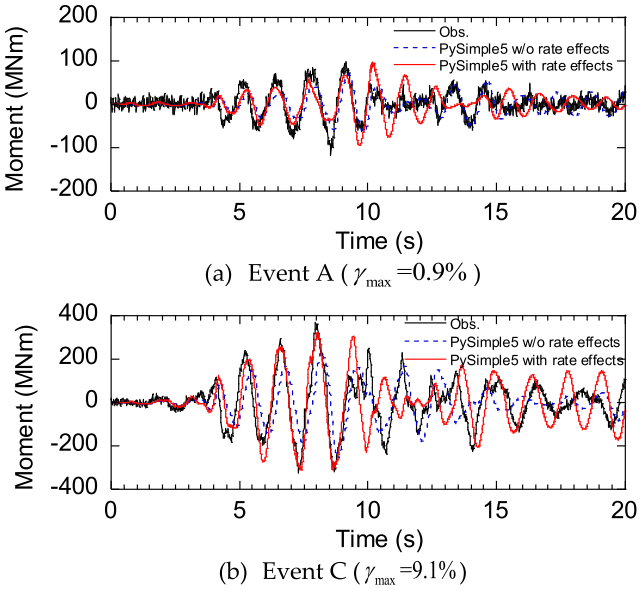

Fig. 13. Comparisons of measured and predicted bending moment time histories at depth of 0.76 *m*.

Figs. 15-16 illustrate the predicted and measured seismic responses in terms of the acceleration response spectra of the superstructure and the bending moments of the pile shaft at the instance of maximum pile displacement. It is observed that the equivalent linear 1D model can only favorably predict Event A, whose maximum shear strain is less than 1%, and that it significantly underestimates Event C, whose maximum shear strain is much larger than 1%. Although the modulus reduction and damping curves are applied in the equivalent linear 1D model, the shear modulus and damping corresponding to an equivalent shear strain, that equals 0.65 times the maximum shear strain, are used to calculate the values of spring stiffness and dashpot damping. This kind of linearization is the source of inaccuracy when it is utilized for cases with large shear strain levels. PySimple1 is also demonstrated in Figs. 15-16. It is found that PySimple1 significantly underestimates Event C since it does not match the shear modulus reduction and damping curves and ignores the rate effect of the soil. These effects are clearly observed in Fig. 17(b), in which the maximum pile displacements are underestimated by PySimple1 and the equivalent linear 1D model. It should be noted that there are no displacement data in these centrifuge tests.

In order to quantify the agreements between the predictions by the models and those by the experiments, the validation metric (see Schatzmann and Olessen, 2010; Oettl, 2015) is introduced and presented by a hit rate, q, and defined as.

$$q = \frac{1}{N}\sum_{i=1}^{N} n_i, \text{ with } n_i = \begin{cases} 1, & \left|\frac{y_i - x_i}{x_i}\right| \leqslant D_q \text{ or } |y_i - x_i| \leqslant W_q \\ 0, & \text{else} \end{cases} \tag{29}$$

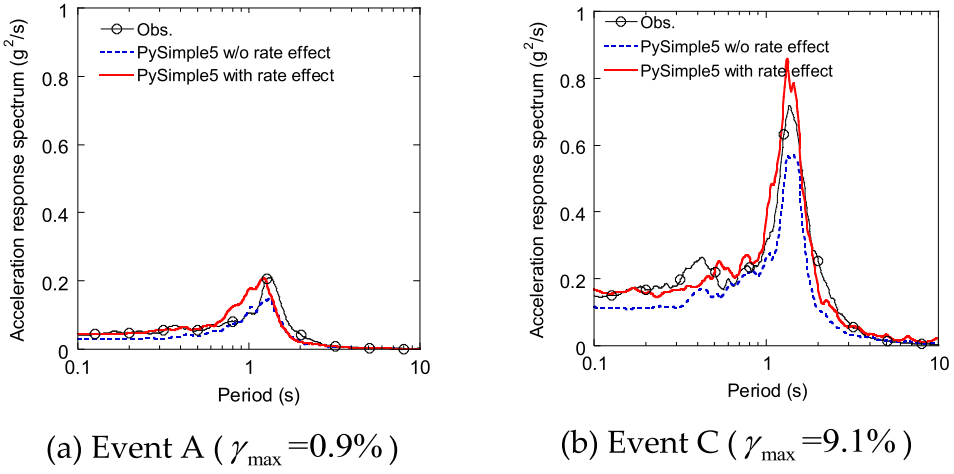

Fig. 12. Comparisons of predicted and measured acceleration response spectra of superstructure with damping of 5%.

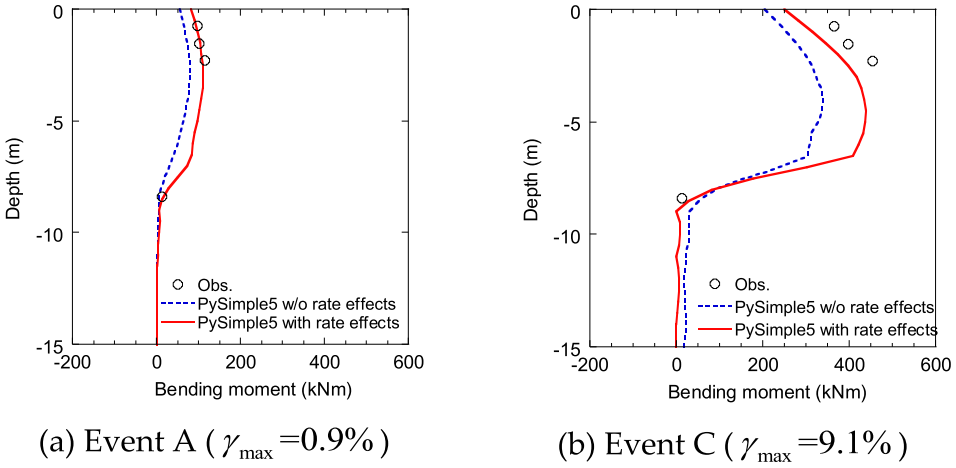

Fig. 14. Comparisons of measured and predicted bending moment profiles at instance of maximum pile displacement for different maximum soil shear strain levels.

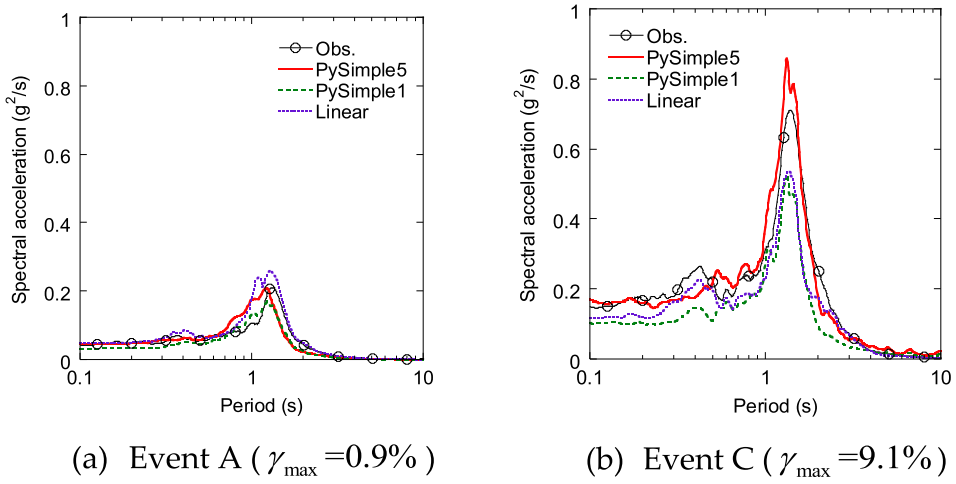

Fig. 15. Comparisons of predicted and measured acceleration response spectra of superstructure with damping of 5%.

where x_i and y_i are the values from the experiments and the predictions, respectively. N is the total number of data, D_q and W_q are the thresholds. The values of the metric, corresponding to the complete agreement and disagreement, are $q = 1$ and $q = 0$, respectively. As suggested by Schatzmann and Olessen (2010) and Oettl (2015), thresholds $D_q = 0.25$ and $W_q = 0.1|\max|$ are used in this study, in which $|\max|$ is a maximum value supposed in the observation. Figs. 18-19 show the scatter plots for a comparison between the predictions and the experiments for the acceleration responses of the superstructure with the damping of 5% and bending moments of the pile shaft at the instance of the maximum pile displacement, together with the corresponding validation metric boundary. It is observed that the proposed model provides a better performance than the equivalent linear 1D model or PySimple1 model, especially in capturing the amplitude in Event C.

3.3. Validation of PyLiq5 for single pile in liquefiable soil

PyLiq5 is validated by the centrifuge test performed by Wilson (1998) for a single pile in liquefiable soil (referred to as CSP2). The schematic of centrifuge test CSP2 is given in Fig. 20. The soil profile in the CSP2 test consists of a top layer of saturated loose sand and a bottom layer of saturated medium dense sand. The depths of the loose and dense sand layers are 9.1 m and 11.4 m, respectively. The relative density of the loose sand is 35% and that of the medium dense sand is 75%. The friction angle of the loose sand is 29.5° and that of the medium dense sand is 38°. The effective unit weights of the loose and medium dense sands are 7.41 kN/m^3 and 9.81 kN/m^3, respectively. The soil parameters for the loose and medium dense sands in the CSP2 test are summarized in Table 5, in which the S-wave velocities (V_s) are determined following

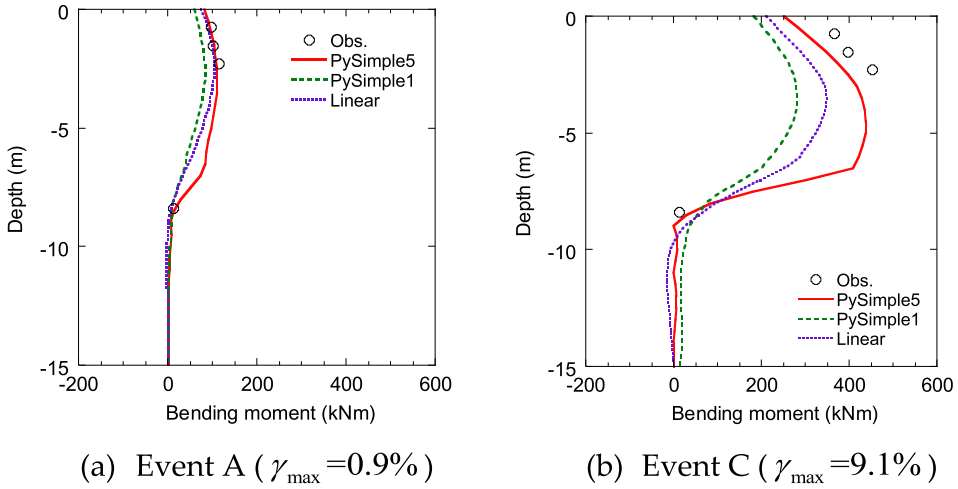

Fig. 16. Comparisons of predicted and measured bending moments of pile shaft at instance of maximum pile displacement for different maximum soil shear strain levels.

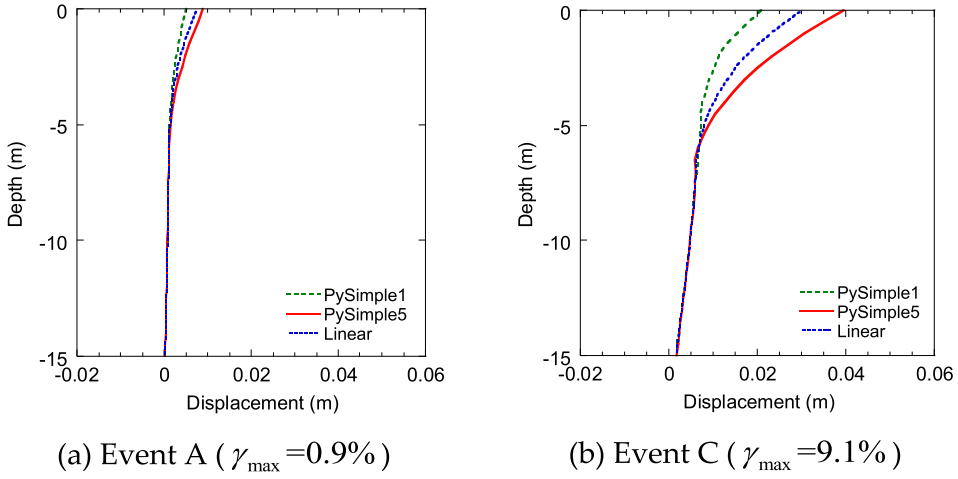

Fig. 17. Comparisons of maximum pile displacements predicted by three models for different maximum soil shear strain levels.

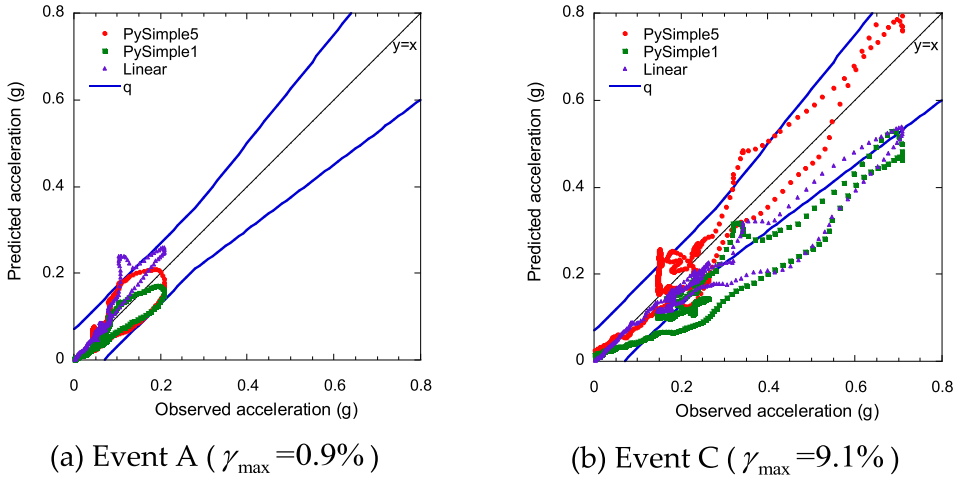

Fig. 18. Scatter plots for comparison between predicted and measured acceleration responses of superstructure with damping of 5%.

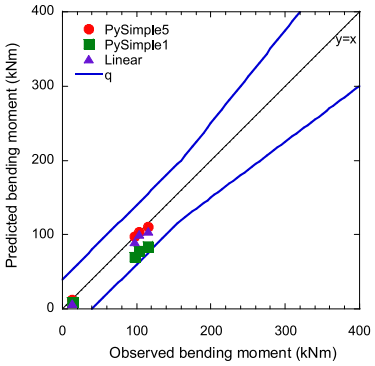

(a) Event A (γ_{max} =0.9%)

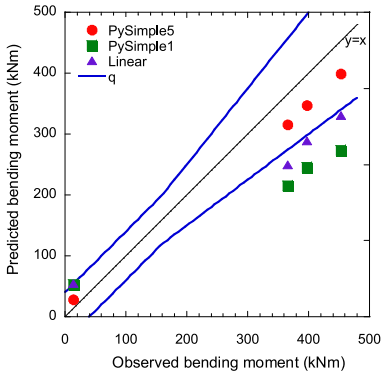

(b) Event C (γ_{max} =9.1%)

Fig. 19. Scatter plots for comparison between predicted and measured bending moments at instance of maximum pile displacement.

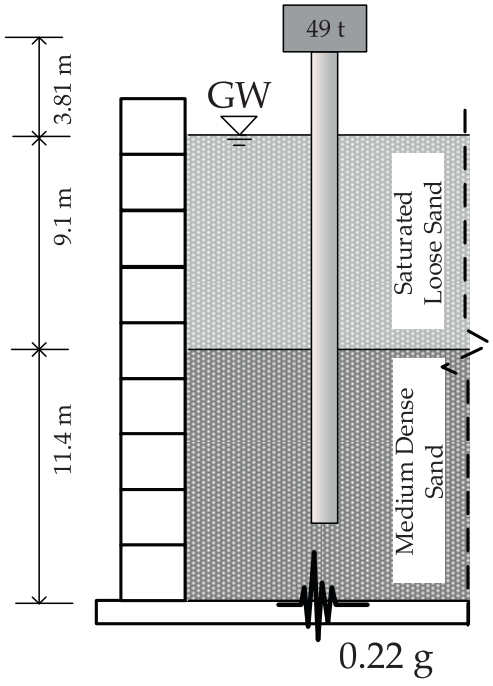

Fig. 20. Schematic of CSP2 centrifuge test.

Brandenberg et al. (2013). The single pile is equivalent to a steel pipe pile with a diameter of 67 cm, a wall thickness of 1.9 cm, and an embedded length of about 16.8 m in the prototype scale, which is extended 3.81 m above the ground surface to carry a superstructure load of 480.2 kN. The imposed excitation at the model base is the scaled Kobe seismic waves with the amplitudes of 0.22 g for Event F, as shown in Fig. 21. The modulus reduction and damping curves for both Nevada sands are assumed to follow the H-D model with parameters $\gamma_{0.5} = 0.1\%$, $h_{max} = 21\%$. The calculations of the ultimate capacity for sand use the formulae in Gerolymos and Gazetas (2006).

The liquefiable soil-pile interaction analysis also includes the site response analysis and the pile response analysis. In this study, OpenSees is used for the site response analyses since the CSP2 test has been simulated well using PressureDependMultiYield2 material for the liquefiable soil with the parameters shown in Table 6 (see Patra and Haldar, 2021).

Fig. 22 illustrates comparisons of the predicted and measured site acceleration responses at the depths of 2.82 m and 13.9 m. It is observed that the predictions match the experimental data well for both depths, although some peaks are not captured at the depth of 2.82 m, which may be due to the low permeability used in the site response analysis. Fig. 23 presents the pore water pressure time histories at the depths of 7.4 m and 12 m. The line of black circles represents the measured results, the red

Table 5
Soil parameters of CSP2 centrifuge test.

Soil layer	Depth of layer top	γ(kN/m^3)	D_r(%)	ϕ(degree)	V_s(m/s)
Loose Nevada sand	0	17.2	35	29.5	177
Dense Nevada sand	9.1	19.6	75	38	235

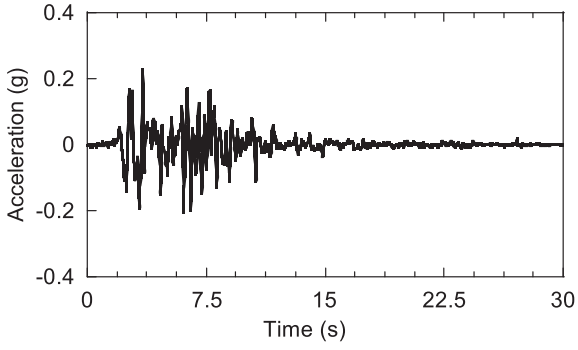

Fig. 21. Time histories of imposed acceleration in CSP2 test.

Table 6
Soil properties for PressureDependMultiYield2 (after Patra and Haldar, 2021).

Parameter	Loose Nevada sand	Dense Nevada sand
Relative density D_r (%)	35	75
Mass density (kg/m^3)	1720	1960
Low-strain shear modulus G_{max} (kPa) at effective confinement of 80 kPa	55e3	110e3
Permeability k (m/s)	6.05e-5	3.7e-5
Friction angle ϕ (degrees)	29.5	38
Phase transformation angle ϕ_{PT} (degrees)	25.5	26
Peak shear strain γ_{max} at 100 kPa mean effective Confinement	0.1	0.1
Contraction parameter c1	0.045	0.013
Contraction parameter c3	0.15	0.0
Dilatation parameter d1	0.06	0.3
Dilatation parameter d3	0.15	0.0
Liquefaction parameter l1	1.0	0
Liquefaction parameter l2	1.0	0
Initial void ratio e	0.70	0.55

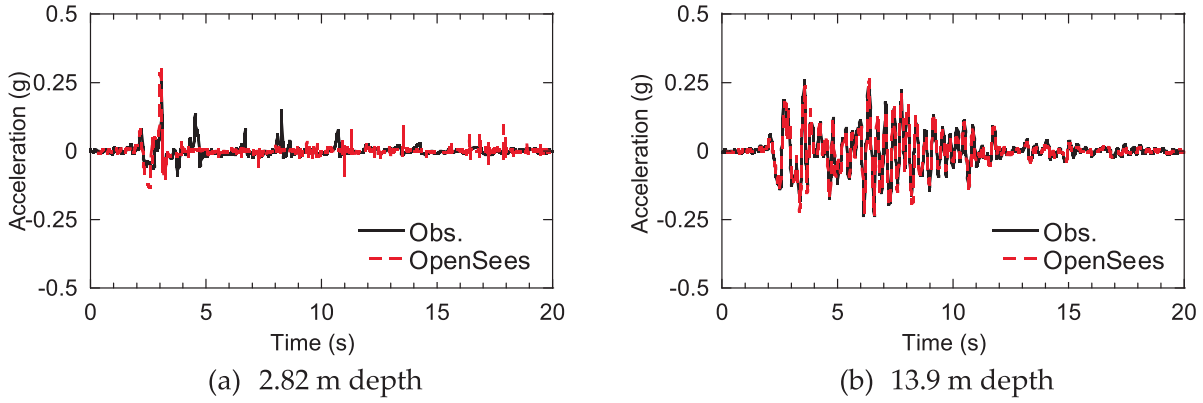

Fig. 22. Comparisons of predicted and measured acceleration time histories at various depths.

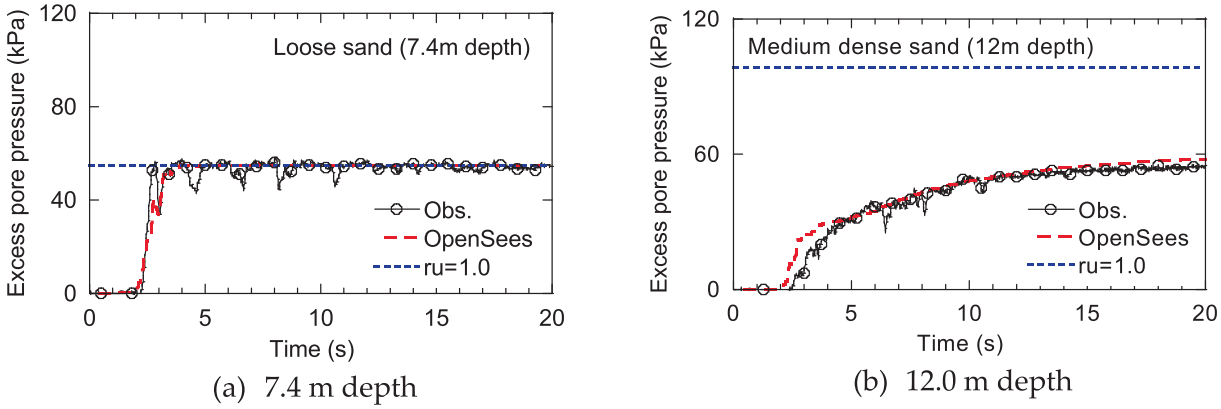

Fig. 23. Comparisons of predicted and measured excess pore pressure time histories.

dashed line represents the predicted pore water pressure levels, and the blue dotted line represents the excess pore pressure ratio, $r_u = 1$, which is the indicator of liquefaction potentiality. It can be seen that the predicted pore water pressure levels are very close to those of the experiments. It can also be seen that the top loose sand layer starts to liquefy after 2 $\sim$ 3 s, while the bottom dense sand layer does not liquefy at all. It is noted that the pore water pres-

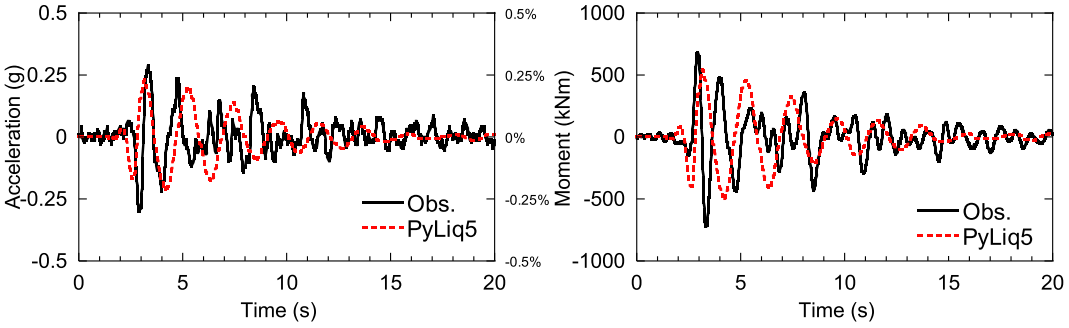

(a) Acceleration time history at pile head (b) Moment time history at 0.76 m

Fig. 24. Comparisons of predicted and measured acceleration and moment time histories.

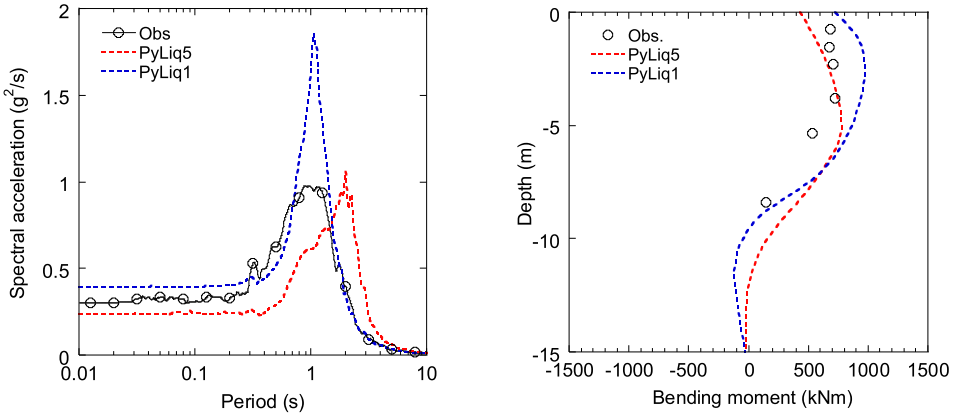

(a) Acceleration response spectra (b) Bending moments

Fig. 25. Comparisons of predicted and measured acceleration response spectra for pile head with damping of 5% and bending moments of pile shaft at instance of maximum bending moment of pile.

sure fluctuates in the experimental results, but the fluctuation is not obvious in the predictions, which may be due to the low permeability used in the site response analysis.

Fig. 24 shows comparisons of the predicted and measured acceleration time histories at the pile head and moment time histories at 0.76 m. Fig. 25 plots comparisons of the predicted and measured acceleration response spectra at the pile head and bending moments of the pile shaft at the instance of maximum bending moment of pile. It is observed that the predictions by PyLiq5 agree reasonably well with the experiments for both the pile head acceleration and pile bending moment, while PyLiq1 overestimates the acceleration response spectra at the pile head and bending moment of the pile shaft for the layered liquefiable soils since the predicted maximum shear forces and pile displacement by PyLiq1 is larger than those by Pyliq5. It is seen that PyLiq5 captures the peak spectral acceleration well, but slightly overestimates the eigen period. This may be due to the calculations of the ultimate capacity for sand, done using the formulae in Gerolymos and Gazetas (2006), which may be not accurate enough.

4. Conclusion

In this study, a new p-y model was proposed for the seismic analyses of piles in non-liquefiable and liquefiable soils. The seismic loading on the pile foundations was investigated using the Beam on Nonlinear Winkler Foundation (BNWF) method and validated by centrifuge tests on a single pile. The conclusions are summarized as follows:

- The proposed PySimple5 model matches the desired modulus reduction curve by identifying three parameters in a hyperbolic function and a linear function using GA, and fits the desired damping curve by applying the Ishihara-Yoshida rule that controls the unloading–reloading curves iteratively through the three parameters, while the previous models do not match these

curves. The rate effect is also considered in PySimple5 by exerting influence on the ultimate capacity and maximum material damping.

- For a single pile in non-liquefiable soil, the superstructure acceleration and pile bending moment predicted by PySimple5 agree well with those obtained from centrifuge tests for different soil shear strain levels, while the equivalent linear 1D model is only suitable when the maximum soil shear strain is less than 1%. PySimple1 underestimates the superstructure acceleration and pile bending moment since it does not match the modulus reduction and damping curves and ignores the rate effect.
- The pore pressure effect is included in PyLiq5 by relating the ultimate capacity to the mean effective stress. For the pile in liquefiable soil, PyLiq5 shows a favorable agreement with the centrifuge tests in terms of the superstructure acceleration and pile bending moment by considering the pore pressure effect.

Acknowledgements

This research was carried out as part of a joint program funded by Shimizu Corporation, J-POWER, Toshiba Energy Systems & Solutions Corporation, MHI Vestas Offshore Wind Japan and ClassNK. The authors express their deepest gratitude to the concerned parties for their assistance during this study.

Appendix A:. Pseudo-static push-over analysis to verify PySimple5

Darendeli (2001) proposed a model for the normalized modulus reduction curve and the material damping curve based on a comprehensive database of laboratory tests, which can account for various factors that influence the soil behavior, such as the soil type (sand, clay or silt), the mean effective confining pressure (σ_0'), over-consolidation stress ratio (OCR), plasticity index (I_p), loading frequency (f), and number of cycles (N). The Darendeli model is applied to calibrate the finite element model in this study, and was used in Zhang et al. (2021). In the Darendeli framework, the normalized modulus reduction and damping curves are expressed by Eqs. (A1)-(A6). The model parameters recommended in Table 8.11 by Darendeli (2001) are used.

$$\tau = G_{\max}\left(\frac{1}{1+(\gamma/\gamma_r)^a}\right)\gamma \tag{A1}$$

$$D_{\text{soil}} = b\left(\frac{G}{G_{\max}}\right)^{0.1} D_{\text{Masing}} + D_{\min} \tag{A2}$$

$$\frac{G_{\max}}{\sigma'_{\text{ref}}} = \left(30 + \frac{75}{I_p/100 + 0.03}\right)\text{OCR}^{0.5} \tag{A3}$$

$$D_{\text{Masing}} = c_1 D_{\text{Masing},a\,=\,1.0} + c_2 D^2_{\text{Masing},a\,=\,1.0} + c_3 D^3_{\text{Masing},a\,=\,1.0} \tag{A4}$$

$$D_{\min} = (\phi_6 + \phi_7 I_p OCR^{\phi_8})\sigma_0'^{\phi_9}[1 + \phi_{10}\ln(f)] \tag{A5}$$

$$D_{\text{Masing, }a=1.0} = \frac{100}{\pi}\left[4\frac{\gamma - \gamma_r \ln\left(\frac{\gamma+\gamma_r}{\gamma_r}\right)}{\frac{\gamma^2}{\gamma+\gamma_r}} - 2\right] \tag{A6}$$

Here, $c_1 = -1.1143a^2 + 1.8618a + 0.2523$, $c_2 = 0.0805a^2 - 0.0710a - 0.0095$,

$c_3 = -0.0005a^2 + 0.0002a + 0.0003$

$\gamma_r = \left(\phi_1 + \phi_2 I_p O\,C\,R^{\phi_3}\right)\sigma_0'^{\phi_4}, a = \phi_5,$

$b = \phi_{11} + \phi_{12}\ln(N),\ \sigma'_{\text{ref}} = p_a\left(\sigma'_0/p_a\right)^{0.9},\ p_a = 100$ kPa

Zhang et al. (2021) performed a series of finite element analyses using a horizontal slice of a pile Plaxis 3D (Plaxis, 2017), which is applied to verify PySimple5. Fig. A1 illustrates the finite element model. The slice is 1 m in thickness, representing a 1-m pile segment of a long pile. Vertical movement on the top and bottom boundaries of the model is constrained, therefore maintaining a plane strain condition. Due to symmetry, only a half-pile segment is modelled. The lateral extent of the boundaries is selected to be 10 times the pile diameter (D) from the center of the pile. The horizontal force is applied as pressure distributed on the vertical symmetry face of the pile, which is

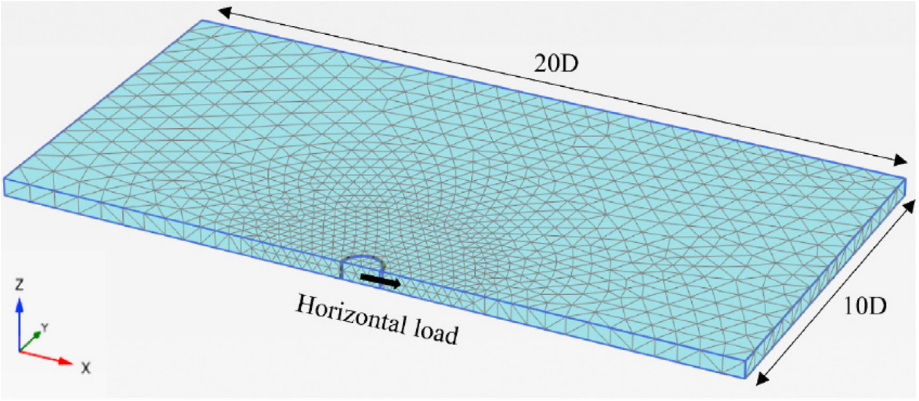

Fig. A1. Three-dimensional finite element model corresponding to single p-y element (After, Zhang et al. 2021).

modelled as a rigid body. The soil-pile interface is simulated by interface elements in Plaxis. Separation between the soil-pile interfaces is not allowed. The tangential property is controlled by the specified interface strength, and relative slip between the pile-soil interface can occur if the mobilised shear stress on the interface reaches the specified limit. In the finite element analyses, the NGI-ADP soil model was used (Grimstad et al. 2012). To ensure that the constitutive relationship of the NGI-ADP model is consistent with the Darendeli shear modulus and damping models, the parameters of the NGI-ADP model shall be fitted to Eqs. (A1)-(A6). In Zhang et al. (2021), a systematical analysis was performed with the parameter space as follows: $\sigma'_0 = 100\ kPa$, $OCR = 1$, $N = 10$, $f = 0.1$ Hz, and $I_p(\%) = 10$, 20, 40, and 60. The procedure for deriving the p-y damping curve from the finite element analyses is provided: 1) The pile is loaded until the load–displacement curve becomes flat, indicating ultimate capacity. 2) The total elastic energy stored in the system is the sum of the elastic energy stored in all the soil elements. For an element i in the finite element model, its elastic stored energy, $E_{S0,i}$, is obtained by calculating the local energy density (stress multiplied by strain) and multiplying it by the volume of the soil element, $V_{el,i}$:

$$E_{S0,i} = V_{el,i}\left(\Sigma\frac{1}{2}\sigma_{kk}\varepsilon_{kk} + \Sigma\frac{1}{2}\tau_{kj}\gamma_{kj}\right) \tag{A7}$$

It is noted that $\gamma_{kj} = \varepsilon_{kj} + \varepsilon_{jk} = 2\varepsilon_{kj}$, with ε_{kj} being the tensorial shear strain output from FEA. The dissipated energy for the same element, $E_{D,i}$, is found by rewriting the equation for the equivalent damping ratio.

$$E_{D,i} = 4\pi D_i E_{S0,i} \tag{A8}$$

where D_i is the soil damping for the considered soil element, obtained from the Darendeli damping curve, at the maximum shear strain of the soil element (i.e., main principal strain-minor principal strain). After finding the potential and dissipated energy for each soil element, the total damping in the soil slice is found by summing up the contributions from all elements.

$$D_{\text{pile\_element}} = \frac{1}{4\pi}\frac{\Sigma E_{D,i}}{\Sigma E_{S0,i}} \tag{A9}$$

Fig. A2 compares the normalized backbone curves and damping curves between the element-level finite element analysis and the BNWF model with the PySimple5. The parameters of PySimple5 are identified by Eqs. (A1)-(A6) for the same parameter space ($\sigma'_0 = 100\ kPa$, $OCR = 1$, $N = 10$, $f = 0.1$ Hz, and $I_p(\%) = 10$, 20, 40, and 60). It is observed that PySimple5 matches well with the finite element analyses in terms of the backbone curve and damping curve for different plastic indexes.

In addition, Zhang et al. (2021) also performed a series of finite element analyses using a 3D finite element model of a full-length pile foundation in Plaxis 3D, which is used to validate the BNWF model with PySimple5. The method for evaluating foundation damping from the FEA results is the same as described above, while the method to integrate system damping from the BNWF model is given in Eqs. (A10)-(A13), which is extended from Zhang et al. (2021) by including the effects of the rotational springs for the modal damping of the soil-pile system, as mentioned in Wang and Ishihara (2022). The simulated pile has a diameter of 2.14 m and a wall thickness of 60 mm. The soil profile is idealized to have a constant undrained shear strength of 20 kPa with depth. The stress–strain and damping responses of the soil follow those defined earlier for a clay with $OCR = 1$ and $I_p(\%) = 60$. The pile is embedded 40 m into the soil and a horizontal force is applied at the pile head. The soil-pile interface is assumed to be fully rough and non-separating.

$$(E_{Soil,i})_{p-y} = \frac{1}{2}p_i y_i,\ (E_{Soil,i})_{m-\theta} = \frac{1}{2}m_i\theta_i \tag{A10}$$

$$(E_{D,i})_{p-y} = 4\pi d_i (E_{Soil,i})_{p-y},$$
$$(E_{D,i})_{m-\theta} = 4\pi d_i (E_{Soil,i})_{m-\theta} \tag{A11}$$

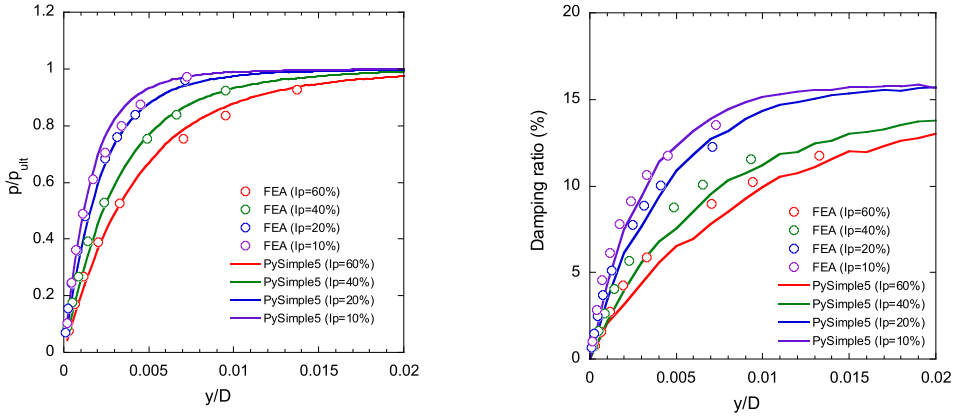

(a) Normalized backbone curve **(b)** Damping curve

Fig. A2. Comparisons of normalized backbone curve and damping curve between PySimple5 and element-level finite element analyses.

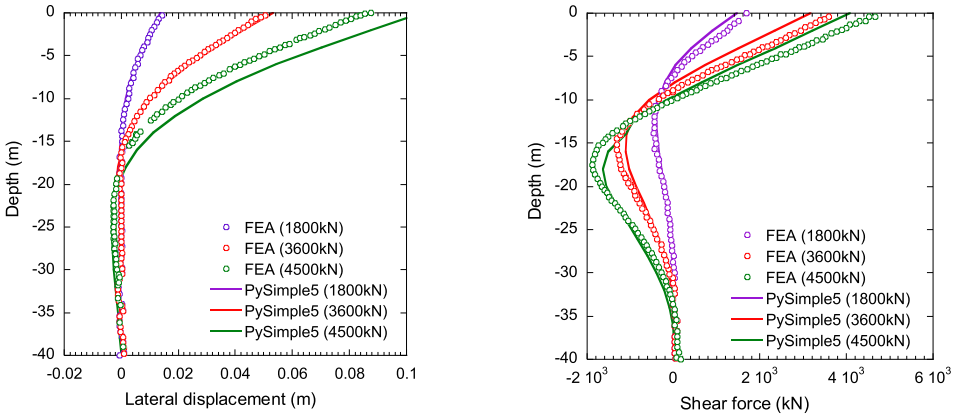

(a) Lateral displacement (m) **(b)** Shear force (kN)

Fig. A3. Comparisons of lateral displacement and shear force of pile calculated by FEA and those by BNWF model with PySimple5.

$$E_{Pile,i} = \frac{1}{2} M_i \Delta\theta_i \tag{A12}$$

$$d_{pile} = \frac{1}{4\pi} \frac{\sum_{i=1}^{n} (E_{D,i})_{p-y} + (E_{D,i})_{m-\theta}}{\sum_{i=1}^{n} \left((E_{Soil,i})_{p-y} + (E_{Soil,i})_{m-\theta} + E_{Pile,i} \right)} = \frac{\sum_{i=1}^{n} d_i \left((E_{Soil,i})_{p-y} + (E_{Soil,i})_{m-\theta} \right)}{\sum_{i=1}^{n} \left((E_{Soil,i})_{p-y} + (E_{Soil,i})_{m-\theta} + E_{Pile,i} \right)} \tag{A13}$$

where $(E_{Soil,i})_{p-y}$ is the stored elastic energy for the *ith* lateral soil spring, p_i is the spring force of the *ith* spring, mobilized at lateral displacement y_i, $(E_{Soil,i})_{m-\theta}$ is the stored elastic energy for the *ith* rotational soil spring, m_i is the spring force of the *ith* spring, mobilized at rotational displacement θ_i, $(E_{D,i})_{p-y}$ is the dissipated energy at the *ith* lateral soil spring, $(E_{D,i})_{m-\theta}$ is the dissipated energy at the *ith* rotational soil spring, and d_i is the damping ratio determined according to the lateral displacement of the spring. For the *ith* pile segment (enclosed between the *ith* and $(i+1)th$ soil springs), $E_{Pile,i}$ is the stored elastic energy, M_i is the cross-sectional bending moment at the *ith* soil spring, and $\Delta\theta_i$ is the difference in cross-section rotation between the *ith* and $(i+1)th$ soil spring. d_{pile} represents the damping for the entire pile system.

A pseudo-static push-over analysis is performed to simulate the maximum cyclic pile response, in which the soil is assumed to have a constant cyclic shear strength and cyclic stress–strain behavior over the pile length. This is an idealized condition, but it demonstrates the rationality of PySimple5 by integrating the soil damping along the entire pile to obtain the correct system damping ratio at the pile head. Fig. A3 compares the pile responses calculated by FEA and the BNWF model with PySimple5 at three different load levels in terms of lateral deflection and cross-section shear force versus depth. The favorable match between FEA and PySimple5 is achieved. Fig. A4 compares the foundation damping ratio evaluated from FEA

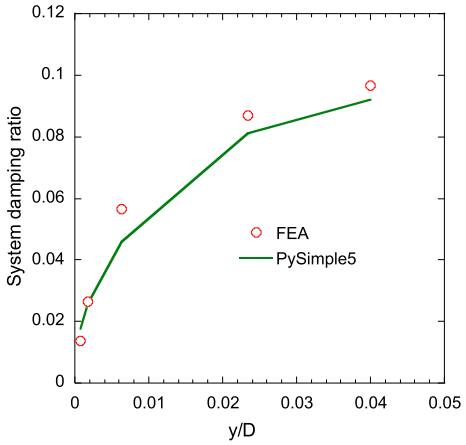

Fig. A4. Comparison of foundation damping ratios calculated by FEA and BNWF model with PySimple5.

of the entire pile versus the damping evaluated from the BNWF model with PySimple5 at five different load levels. It is noticed that the two predictions are close, although the foundation damping ratio integrated from the BNWF model with PySimple5 is slightly lower than that evaluated from FEA. The difference is believed to be due to the interaction between the slices, which is not captured in the BNWF model.

References

Afacan, K.B., Brandenberg, S.J., Stewart, J.P., 2014. Centrifuge modeling studies of site response in soft clay over wide strain range. J. Geotech. Geoenviron. Eng. 140 (2), 04013003.

Afacan, K.B., Yniesta, S., Shafiee, A., Stewart, J.P., Brandenberg, S.J., 2019. Total stress analysis of soft clay ground response in centrifuge models. J. Geotech. Geoenviron. Eng. 145 (10), 04019061.

API RP 2A-WSD, 2010. Recommended Practice for Planning. Designing and Constructing Fixed Offshore Platforms, American Petroleum Institute.

Boulanger, R.W., Curras, C.J., Kutter, B.L., Wilson, D.W., Abghari, A., 1999. Seismic soil-pile-structure interaction experiments and analyses. J. Geotech. Geoenviron. Eng. 125 (9), 750–759.

Bowles, J.E., 1993. Foundation analysis and design, 5th edition. The McGraw-Hill Companies Inc.
Brandenberg, S.J., Boulanger, R.W., Kutter, B.L., Chang, D., 2005. Behavior of pile foundations in laterally spreading ground during centrifuge tests. J. Geotech. Geoenviron. Eng. 131 (11), 1378–1391.
Brandenberg, S.J., Zhao, M., Boulanger, R.W., Wilson, D.W., 2013. p-y plasticity model for nonlinear dynamic analysis of piles in liquefiable soil. J. Geotech. Geoenviron. Eng. 139 (8), 1262–1274.
Brown, M.J., 2004. The rapid load testing of piles in fine grained soils. University of Sheffield PhD Thesis.
Butt, U.A., Ishihara, T., 2012. Seismic load evaluation of wind turbine support structures considering low structural damping and soil structure interaction. In: Proceedings of the European Wind Energy Association Annual Event. Copenhagen, Denmark.
Choi, J.I., Kim, M.M., Brandenberg, S.J., 2015. Cyclic p-y plasticity model applied to pile foundations in sand. J. Geotech. Geoenviron. Eng. 141 (5), 04015013.
d'Onofrio, A., Silvestri, F., Vinale, F., 1999. Strain rate dependent behaviour of a natural stiff clay. Soils Found. 39 (2), 69–82.
Darendeli, M.B., 2001. Development of a new family of normalized modulus reduction and material damping curves. The University of Texas at Austin.
Dash, S., Rouholamin, M., Lombardi, D., Bhattacharya, S., 2017. A practical method for construction of py curves for liquefiable soils. Soil Dyn. Earthquake Eng. 97, 478–481.
DNVGL-RP-C212, 2017. Offshore soil mechanics and geotechnical engineering. DNV, Oslo, Norway.
Gerolymos, N., Gazetas, G., 2006. Development of Winkler model for static and dynamic response of caisson foundations with soil and interface nonlinearities. Soil Dyn. Earthquake Eng. 26 (5), 363–376.
Grimstad, G., Andresen, L., Jostad, H.P., 2012. NGI-ADP: Anisotropic shear strength model for clay. Int. J. Numer. Anal. Methods Geomech. 36 (4), 483–497.
Harukigaoka Wind Power Co., Ltd., 2018. Accident survey report, https://www.meti.go.jp/shingikai/sankoshin/hoan_shohi/denryoku_anzen/newenergy_hatsuden_wg/pdf/009_05_00.pdf.
Hölscher, P., Van Tol, A.F., Huy, N.Q., 2012. Rapid pile load tests in the geotechnical centrifuge. Soils Found. 52 (6), 1102–1117.
IEC61400-6, 2000. Wind energy generation systems –Part 6: Tower and foundation design requirements. International Electrotechnical Commission.
Ishihara, K., Yoshida, N., Tsujino, S., 1985. Modelling of stress-strain relations of soils in cyclic loading. In: International Conference on Numerical Methods in Geomechanics, pp. 373–380.
Ishihara, T., 2010. Guidelines for Design of Wind Turbine Support Structures and Foundations (In Japanese).
Kagawa, T., Kraft Jr., L.M., 1980. Seismic p∼y Responses of Flexible Piles. Journal of the Geotechnical Engineering Division 106 (8), 899–918.
Krathe, V.L., Kaynia, A.M., 2017. Implementation of a non-linear foundation model for soil-structure interaction analysis of offshore wind turbines in FAST. Wind Energy 20 (4), 695–712.
Lai, Y., Wang, L., Zhang, Y., Hong, Y., 2021. Site-specific soil reaction model for monopiles in soft clay based on laboratory element stress-strain curves. Ocean Eng. 220 108437.
Maranha, J.R., Pereira, C., Vieira, A., 2016. A viscoplastic subloading soil model for rate-dependent cyclic anisotropic structured behaviour. Int. J. Numer. Anal. Methods Geomech. 40 (11), 1531–1555.
Markou, A.A., Kaynia, A.M., 2018. Nonlinear soil-pile interaction for offshore wind turbines. Wind Energy 21 (7), 558–574.
Masing G., 1926. Eigenspannungen und verfestigung beim messing (Self stretching and hardening for brass), In: Proceedings of the Second International Congress for Applied Mechanics, Zurich, Switzerland, pp. 332-335 (in German).
Matlock, H., 1970. Correlation for design of laterally loaded piles in soft clay. In: Offshore Technology Conference. OnePetro.
Matlock, H., Foo, S.H.C., Bryant, L.M., 1978. Simulation of lateral pile behavior under earthquake motion. In: From Volume I of Earthquake Engineering and Soil Dynamics–Proceedings of the ASCE Geotechnical Engineering Division Specialty Conference, June 19-21, 1978, Pasadena, California.
Mazzoni, S., McKenna, F., Scott, M.H., Fenves, G.L., 2006. OpenSees command language manual. Pacific Earthquake Engineering Research (PEER) Center 26 (4), 137–158.
Oettl, D., 2015. Quality assurance of the prognostic, microscale wind-field model GRAL 14.8 using wind-tunnel data provided by the German VDI guideline 3783–9. J. Wind Eng. Ind. Aerodyn. 142, 104–110.
Patra, S.K., Haldar, S., 2021. Seismic response of monopile supported offshore wind turbine in liquefiable soil. Structures. 31, 248–265.
Plaxis. 2017. Plaxis 3D reference manual 2017.
Popescu, R., Prevost, J.H., 1993. Centrifuge validation of a numerical model for dynamic soil liquefaction. Soil Dyn. Earthq. Eng. 12, 73–90.
Rahmani, A., Taiebat, M., Finn, W.D.L., Ventura, C.E., 2018. Evaluation of p-y springs for nonlinear static and seismic soil-pile interaction analysis under lateral loading. Soil Dyn. Earthquake Eng. 115, 438–447.
Randolph, M.F., 1992. Dynamic and static soil models for axial pile response. In: Proceedings of the 4th International Conference on Application of Stress-wave Theory to Piles, pp. 3–14.
Schatzmann, M., Olesen, H., F.j., 2010. COST 732 model evaluation case studies: approach and results. COST Off, Brussels, p. 121.
Sheahan, T.C., Ladd, C.C., Germaine, J.T., 1996. Rate-dependent undrained shear behavior of saturated clay. Journal of Geotechnical Engineering 122 (2), 99–108.
Wang, L., Ishihara, T., 2020. A study of the effects of foundation uplift on the seismic loading of wind turbine tower and shallow foundation using a new dynamic Winkler model. Eng. Struct. 219 110745.
Wang, L., Ishihara, T., 2022. A semi-analytical one-dimensional model for offshore pile foundations considering effects of pile diameter and aspect ratio. Ocean Eng. 250 110874.
Wang, L., Lai, Y., Hong, Y., Mašín, D., 2020. A unified lateral soil reaction model for monopiles in soft clay considering various length-to-diameter (L/D) ratios. Ocean Eng. 212 107492.
Wilson, D.W., 1998. Soil-pile-superstructure interaction in liquefying sand and soft clay. University of California, Davis PhD Thesis.
Yniesta, S., Brandenberg, S.J., Shafiee, A., 2017. ARCS: A one dimensional nonlinear soil model for ground response analysis. Soil Dyn. Earthquake Eng. 102, 75–85.
Yniesta, S., Janati-Idrissi, M., 2021. Integration of viscoplastic effects in a one-dimensional constitutive model for ground response analysis. Can. Geotech. J. 58 (4), 468–478.
Yoo, M.T., Choi, J.I., Han, J.T., Kim, M.M., 2013. Dynamic p-y curves for dry sand from centrifuge tests. J. Earthquake Eng. 17 (7), 1082–1102.
Zhang, Y., Andersen, K.H., 2017. Scaling of lateral pile py response in clay from laboratory stress-strain curves. Mar. struct. 53, 124–135.
Zhang, Y., Aamodt, K.K., Kaynia, A.M., 2021. Hysteretic damping model for laterally loaded piles. Mar. struct. 76 102896.